AD-A083 726 PENNSYLVANIA STATE UNIV UNIVERSITY PARK MATERIALS RE--ETC F/6 11/4
COMPOSITE PYROELECTRIC MATERIALS.(U)
JUN 79 R E NEWNHAM, A S BHALLA N00014-78-C-0291

UNCLASSIFIED NL

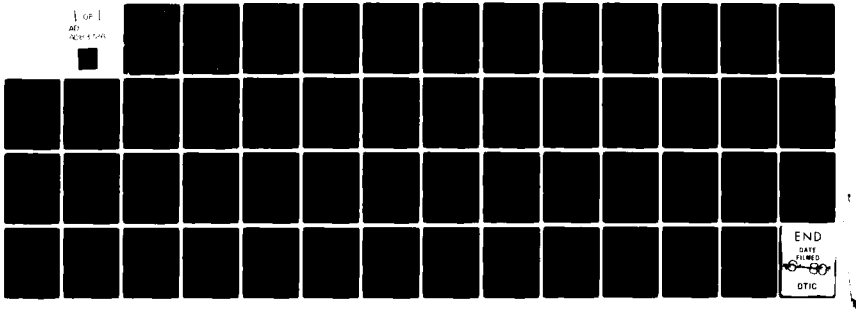

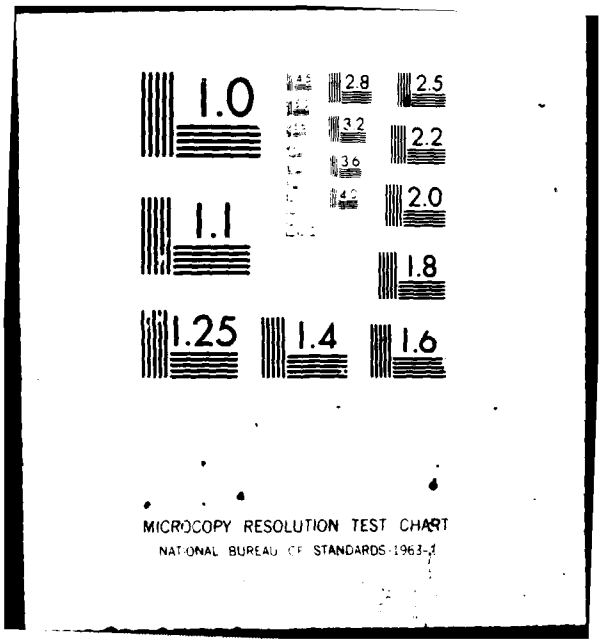
1.0
2.8
2.5
3.2
2.2
3.6
2.0
1.1
1.8
1.25
1.4
1.6
MICROCOPY RESOLUTION TEST CHART
NATIONAL BUREAU OF STANDARDS-1963-A

COMPOSITE PYROELECTRIC MATERIALS,

FINAL TECHNICAL REPORT.

Jul 78-30 Sep 79,

Contract Period July 1, 1978 to June 30, 1979

by

30 Jun 79

R.E. Newnham A.S. Bhalla

Materials Research Laboratory
The Pennsylvania State University
University Park, Pennsylvania 16802

(814)865-1612

This research was sponsored by the Defense Advanced Research Projects Agency under ARPA Order No. 3617 Contract No. MDA903-78-C-0306 monitored by Lynn Garn, Night Vision and Electro-Optics Laboratory.

N00014-78-C-0391

The views and conclusions contained in this document are those of the author and should not be interpreted as necessarily representing the official policies either express or implied of the Defense Advanced Research Projects Agency or the United States Government.

THE MATERIALS RESEARCH LABORATORY

THE PENNSYLVANIA STATE UNIVERSITY

UNIVERSITY PARK, PENNSYLVANIA

TABLE OF CONTENTS

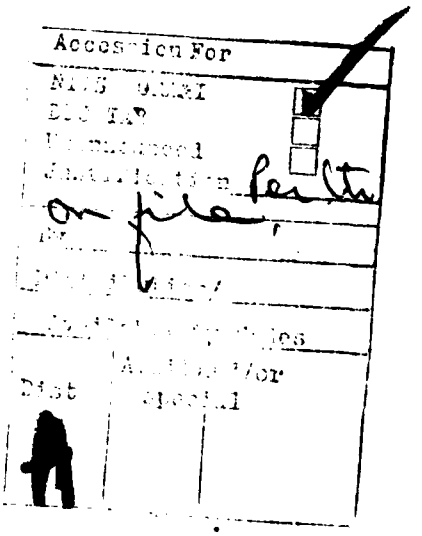

Report Summary

Pyroelectric materials develop electric charge with temperature change. They are used in thermal device applications such as surveillance, burglar alarms and vidicon night-image systems. Greater pyroelectric sensitivity is needed for many vidicon applications. We are exploring ways of increasing the pyroelectric figure-of-merit (pyroelectric coefficient/permittivity) through the use of composite materials.

In this report we discuss the results of work carried out at Penn State and at the North American Philips Laboratory (Dr. J. Dougherty and Dr. W. Smith). The design principles and experimental data for a model system are described in the section entitled Pyroelectric PZT Composites. For PZT-Spurrs composites with parallel connectivity, the pyroelectric figure-of-merit is more than five times larger than for a poled PZT ceramic.

Further improvement is possible by utilizing the secondary pyroelectric effect arising from thermal expansion mismatch in the composite. Secondary pyroelectric effects can be very large, as discussed in Appendix I.

Two very interesting ferroelectrics with substantial pyroelectric effects are antimony sulfur iodide (SbSI) and the boracites, typified by $Fe_3B_7O_{13}I$. Pyroelectric measurements are reported in Appendices II and III. SbSI single crystals and boracite-plastic composites both have extremely large pyroelectric effects, comparable to the best vidicon materials.

Pyroelectric PZT Composites

1. Introduction

Pyroelectric materials are of interest in thermal device applications[1] such as thermal image systems (vidicons), forest fire mapping, surveillance, burglar alarms, medical thermography, testing semiconductor integrated circuits, and energy-saving applications (locating heat losses in homes and factories). Presently, many of these devices are made either from single crystals or ceramic discs of pyroelectric materials. In some of these applications, large target materials are desirable. The availability of such targets is generally restricted by the small size of the single crystals and by the low figure of merit of alternative materials. In terms of materials parameters the figure of merit is defined as

$$M_p = \frac{p}{\varepsilon C D} \qquad [1]$$

where p, ε, C and D are the pyroelectric coefficient, the dielectric constant, the volume specific heat, and the lateral thermal diffusivity, respectively. In order to develop more efficient devices, an improvement in the figure of merit of pyroelectric materials is desirable so that the need of large, single crystals can be relaxed. Recently, it has been demonstrated that piezoelectric transducers made of PZT:Polymer composites have superior performance to those made of pure PZT ceramic[2,3]. In this paper we report the fabrication of several PZT composites and compare their pyroelectric performance with normal PZT ceramics.

2. Theoretical Modeling

Under stress-free conditions, the measured pyroelectric coefficient is the sum of the primary and the secondary effect[4] (product of thermal expansion,

piezoelectric and elastic coefficients). For most ferroelectric materials, the primary and secondary coefficients are of opposite sign, lowering the overall pyroelectric response. Clearly, if the piezoelectric response could be modified by suitable clamping, the secondary contribution to the pyroelectric effect can be altered. Thus, by fabricating a diphasic material with an appropriate second component, the pyroelectric coefficient can be changed significantly. It is suggested on the basis of the following models that two-phase composites with suitably chosen modes of phase interconnection (connectivity) can have property combinations that improve the figure of merit for device applications beyond those possible with the individual phases.

2.1 Simple Series Connection

Consider the response of a multilayer diphasic pyroelectric (Fig. 1a) made from a volume fraction ^1v of phase with permittivity $^1\varepsilon_{33}$ and pyroelectric coefficient $^1p_3$, interleaved along the x_3-direction with a phase of volume fraction ^2v, permittivity $^2\varepsilon_{33}$, and pyroelectric coefficient $^2p_3$. Piezoelectric and thermal expansion coefficients are represented by d_{ij} and α_i, respectively. To simplify the calculation we assume that both phases are poled ceramics with conical symmetry and with the polar axis (x_3) perpendicular to the plane of the interleaving layers.

With close transverse connections of thin sheets, and assuming no surface tractions, the total pyroelectric effect ($\bar{p}_3$) is calculated for a uniform temperature change ΔT. There are two terms corresponding to the primary and secondary effects of the composite:

$$\bar{p}_3 = \frac{{}^1v\,{}^1p_{33}\,{}^2\varepsilon_{33} + {}^2v\,{}^2p_3\,{}^1\varepsilon_{33}}{{}^1v\,{}^2\varepsilon_{33} + {}^2v\,{}^1\varepsilon_{33}}$$

$$+ \frac{2\,{}^1v\,{}^2v({}^2\varepsilon_{33}\,{}^1d_{31} - {}^1\varepsilon_{33}\,{}^2d_{31})({}^2\alpha_1 - {}^1\alpha_1)}{({}^1v\,{}^2\varepsilon_{33} + {}^2v\,{}^1\varepsilon_{33})[{}^1v({}^2s_{11} + {}^2s_{12}) + {}^2v({}^1s_{11} + {}^1s_{12})]} \qquad [2]$$

The corresponding electric permittivity is

$$\bar{\varepsilon} = \frac{{}^1\varepsilon\,{}^2\varepsilon}{{}^1v\,{}^2\varepsilon + {}^2v\,{}^1\varepsilon}. \qquad [3]$$

The voltage coefficient is ratio of the pyroelectric coefficient and permittivity.

$$\frac{\bar{p}_3}{\bar{\varepsilon}_{33}} = \frac{{}^1v\,{}^1p_3}{{}^1\varepsilon_{33}} + \frac{{}^2v\,{}^2p_3}{{}^2\varepsilon_{33}} + \frac{2\,{}^1v\,{}^2v({}^2\alpha_1 - {}^1\alpha_1)}{[{}^1v({}^2s_{11} + {}^2s_{12}) + {}^2v({}^1s_{11} + {}^1s_{12})]}$$

$$\times \left(\frac{{}^1d_{31}}{{}^1\varepsilon_{33}} - \frac{{}^2d_{31}}{{}^2\varepsilon_{33}}\right). \qquad [4]$$

The secondary pyroelectric effect of composite arises from thermal expansion mismatch $({}^2\alpha_1 - {}^1\alpha_1)$. This is a good example of a product property[4] since neither phase is required to exhibit primary pyroelectricity. A pyroelectric effect appears even when ${}^1p_3 = {}^2p_3 = 0$.

Secondary pyroelectric effects also appear in a composite with <u>parallel connectivity</u>. In this case, the composite pyroelectric coefficient is

$$\bar{p}_3 = {}^1v\,{}^1p_3 + {}^2v\,{}^2p_3 + \frac{{}^1v\,{}^2v({}^2\alpha_3 - {}^1\alpha_3)({}^1d_{33} - {}^2d_{33})}{{}^1v\,{}^2s_{33} + {}^2v\,{}^1s_{33}} \qquad [5]$$

and the permittivity is given by

$$\bar{\varepsilon} = {}^{1}v\,{}^{1}\varepsilon + {}^{2}v\,{}^{2}\varepsilon. \qquad [6]$$

In many pyroelectric (and piezoelectric) applications, low permittivity is very desirable. This is a problem because the best materials are ferroelectrics with large dielectric constants. To maximize the figure of merit, it would be very helpful to decouple the pyroelectric coefficient from the permittivity. In essence, this means changing form parallel to series connection during the processing steps, and keeping the pyroelectric effect large by making use of the secondary effect which acts through the piezoelectric coefficients and thermal expansion.

2.2 Thermal Conduction

Thermal diffusion causes a crosstalk problem in some pyroelectric device applications, such as vidicons operated at slow panning speeds[1]. Diffusivity is measured by heating one portion of the pyroelectric target and monitoring the electrical response at a position some distance away. Low thermal conductivity within the target is desirable in this regard. Triglycine sulfate and triglycine fluoberyllate are good insulators, but further improvement may be possible with composites. Essentially, this makes use of the reticulation principle proposed by Singer and Lalak[1]. Photolithography followed by etching is used to divide the target into a number of thermally-isolated islands.

The thermal conductivity coefficient k_{ij} relates heat flow to thermal gradient, $h_i = k_{ij}\,(\partial T/\partial x_j)$. In cubic crystals as well as in amorphous and polycrystalline materials, k_{ij} is a scalar so that thermal conduction is isotropic. This is not true for crystals having symmetry lower than cubic, nor is it true for anisotropic composites. Thermal conductivity is a second-rank tensor for composites with series or parallel connection, with principal axes parallel and perpendicular to the layers. By choosing two components with vastly different thermal conductivities (k values range over about five orders

of magnitude), it is possible to incorporate enormous thermal anisotropy in a layered composite. Heat shields are an example. By way of comparison, with the best single phase materials, graphite conducts heat only four times better in the carbon layers than in the perpendicular direction.

2.3 Modification of Electrical Conductivity

One of the important differences between a pyroelectric vidicon and an ordinary vidicon is that the pyroelectric target is an excellent insulator. The build-up of charge on the surface of the pyroelectric eventually prevents the electron beam from landing and operation ceases. To prevent the accumulation of negative charge, a positive charge (referred to as the pedestal current) is supplied to the surface. Several techniques for producing the pedestal current have been tried but none are entirely successful[1]. In the gas method, positive gaseous ions impinge on the target, neutralizing the negative electronic charge. Among the disadvantages of this method is short tube life, noise, and defocussing effects. Another way of producing pedestal current is by secondary electron emission in which electrons are removed from the target by bombardment with energetic electrons. Positive charging is accomplished during the horizontal flyback time while the video is blanked off. This requires a modification of the electronics and also produces less uniform charging than the gas method.

The use of composites suggest another way of eliminating target charge by selected charge leakage. If the conductivity of one phase could be altered at will, it would be possible to adjust the field distribution and flux concentration during the poling process. Afterwards, the resistivity could be changed again to lower the effective permittivity of the composite. A third possible advantage relates to pedestal charge: by altering the resistivity, accumulated charge could be leaked off the target surface.

Control of the conductivity might be accomplished in either the active or inactive component of the pyroelectric composite. Components of interest in this regard are photopolymers, thermopolymers, and ovonic glasses in which conductivity changes occur under irradiation, or by heating, or under electric fields.

3. PZT and PZT:Polymer composites

3.1 Materials

To test some of these ideas we have investigated the pyroelectric characteristics of PZT:polymer composites. The two phases which have been used for the majority of these studies are a commercial PZT (Ultrasonic PZT 501[1]), and a 'hard' plastic casting component ('SPURRS'). The PZT 501 is a proprietary piezoelectric formulation, categorized as a 'soft' donor-doped material used primarily for its high piezoelectric d coefficients. It is not an optimum composition for pyroelectric response, but is a very easy formulation with which to reproduce consistent electrical properties. It appeared well suited to the modeling of composites for pyroelectric evaluation, where the changes in response affected by the composite are of primary interest, rather than the absolute levels.

SPURRS is a complex polymer system which has been developed primarily for casting and replication. It is a multicomponent system[2] in which the mechanical

---

†[1]Ultrasonics Powders Inc., 2383 S. Clinton Ave., South Plainfield, NJ 07080.

†[2]SPURRS: A typical chemical mixture of the following chemicals in the gravimetric ratios:

RD-4 (VCD)	10 gm
D.E.R. 736	4 gm
NSA (nonethyl Succinic) anhydride	26 gm
DMAE (dimethyl amino ethanol)	0.4 gm

Setting time: 8 hours, 70°C.

Source: Ernest F. Fullam, Inc., Schenectady, NY 12301.

and thermomechanical properties can be controlled by adjusting the chemistry and curing temperature. A major advantage of this plastic for the replamine replication work is that the unpolymerized liquid has very low viscosity (60 cps), allowing good vacuum impregnation and a close mating of ceramic:plastic phases in fine-scale replications.

3.2 Sample Preparation

The following samples were prepared.

(1) Pure Ultrasonic PZT 501. Disk-shaped samples of the 501 formulation were prepared by cold pressing the powder and firing under controlled PbO partial pressure. Samples 1 cm diameter and 1 mm thick were fabricated. Sputtered chrome:gold electrodes were applied to the major faces, and the ceramics poled under 14 kv/cm at 90°C for 5 minutes.

Completion of the poling was established by checking the piezoelectric coefficient d_{33} against standard samples. For pyroelectric study, samples were thinned to 200 μm meters by grinding and repolishing; after thinning, all samples were repoled and again checked for consistency of d_{33}.

(2) PZT:Polymer Films. Prefired PZT 501 was ground to a fine powder, then classified to 400 mesh. The powder was then suspended in liquid monomer and the mixture dispersed on a teflon plate to form a thin layer. After curing at 70°C for 8 hours, samples were polished to a thickness of 35 μm meters and poled. The PZT:polymer ratio and the size distribution of PZT particles were determined by optical microscopy.

(3) PZT:Polymer Replamine Samples. Replamine samples were prepared using two coral species, porites goniopera and porites-porites. The porites-porites has a predominantly 3:1 connectivity and were preferred for the replication experiments. Coral templates having a narrow pore size distribution, were used in

making the PZT replica. Using a lost wax method, porous PZT specimens of suitable dimensions were prepared from the templates. Soft polymer adiprin and the hard Spurrs were used for filling the PZT replicas in most of the samples. Variations in hardness of the Spurrs were achieved by altering the polymer composition and curing temperature.

4. Electrical Measurements

In the present studies, emphasis has been placed upon the determination of the parameters $\bar{p}$ and $\bar{\varepsilon}$, the effective average pyroelectric and dielectric constants for the composites, and the resulting ratio $\bar{p}/\bar{\varepsilon}$. Qualitative pyroelectric response was evaluated by the Chynoweth method[5]. Automated quantitative measurements of the pyroelectric coefficients were made by the Byre-Roundy direct method[6].

Dielectric properties were measured at both 1 MHz and 1 KHz. Although the 1 MHz dielectric data provide a better signal-to-noise ratio in the pyroelectric tests, possible piezoelectric resonances nearby in frequency make a 1 KHz dielectric measurement also necessary. For a 755 μm thick PZT 501 disk the permittivity at 1 MHz was found to be 60% of the 1 KHz value. The replamine composites, on the contrary, showed less than 10% dispersion, indicative of the damping effects of the second phase.

5. Results and Discussion

5.1 Pure Ultrasonics 501 PZT

Samples were measured with as-fired surfaces electroded with air drying silver paste and also with polished surfaces electroded with sputtered gold-palladium. No significant differences were found for the two types of electrode. The dielectric constant was found to be quite sensitive to the degree

of poling, showing the highest values in the electrically or thermally depoled state, often dropping by 25% after poling.

When samples were poled at high temperatures and held under dc bias while being cooled to room temperature, the initial heating cycle often showed anomalously large discharge currents originating from thermally-stimulated current (TSC). All graphs of p versus T are for data that were reproducible on temperature cycling.

A base line for the PZT composite system are the properties of pure PZT 501:

$$p = 5\times10^{-4} \text{ coul/m}^2\text{-K}$$

$$\epsilon_r \approx 1600$$

$$p/\epsilon_r = 2.0 - 2.7\times10^{-7} \text{ coul/m}^2\text{-K}.$$

5.2 PZT: Loaded Film

The controlled grit size (35 μm) composite called a "loaded film" has the pyroelectric response of a dilute, pure PZT. The magnitude and temperature dependence of $\bar{p}/\bar{\epsilon}$ are very close to that of the solid PZT disc, while $\bar{p} \approx 5\times10^{-5}$ c/m^2-K and $\bar{\epsilon} \approx 200$ are both reduced by a factor of ten.

5.3 Replamine Composites

(a) PZT:Adiprin. Using the soft plastic, Adiprin, the measured pyroelectric values for the composites are

$$\bar{p} \approx 2.25\times10^{-5} \text{ c/m}^2\text{-K}$$

$$\bar{\epsilon} \approx 60 \text{ (1 MHz)}$$

$$\bar{p}/\bar{\epsilon} \approx 3.2\times10^{-7} \text{ c/m}^2\text{K}.$$

The temperature dependences are shown in Fig. 1. The figure of merit, $\bar{p}/\bar{\epsilon}$,

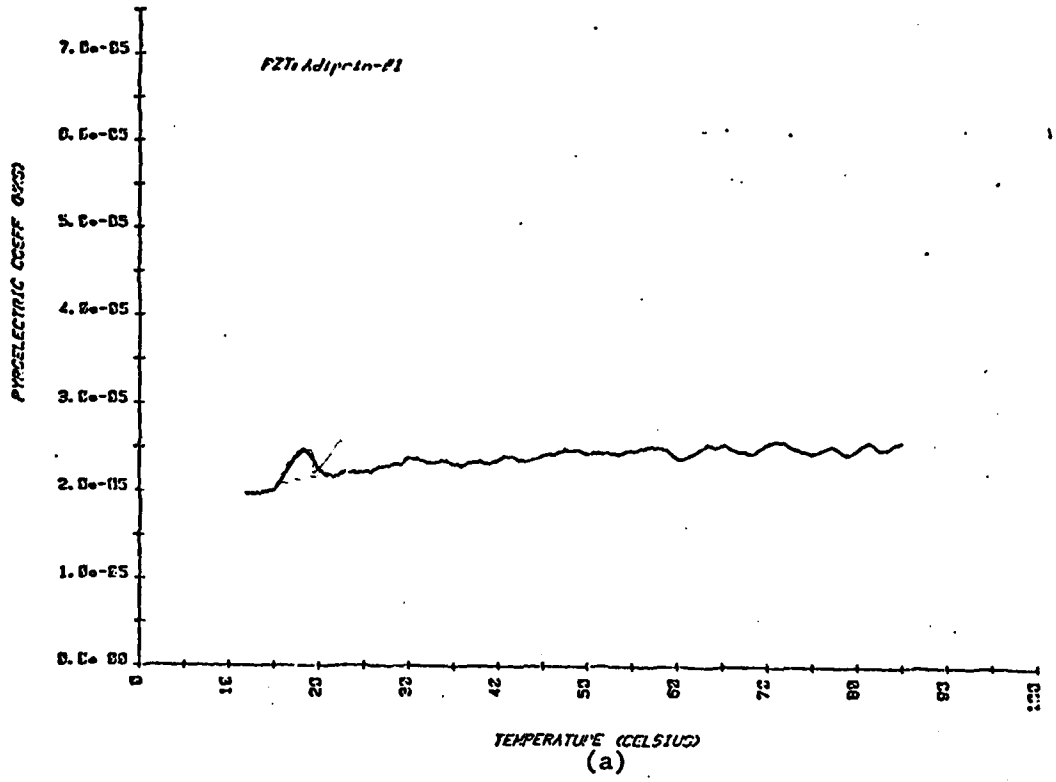

(a)

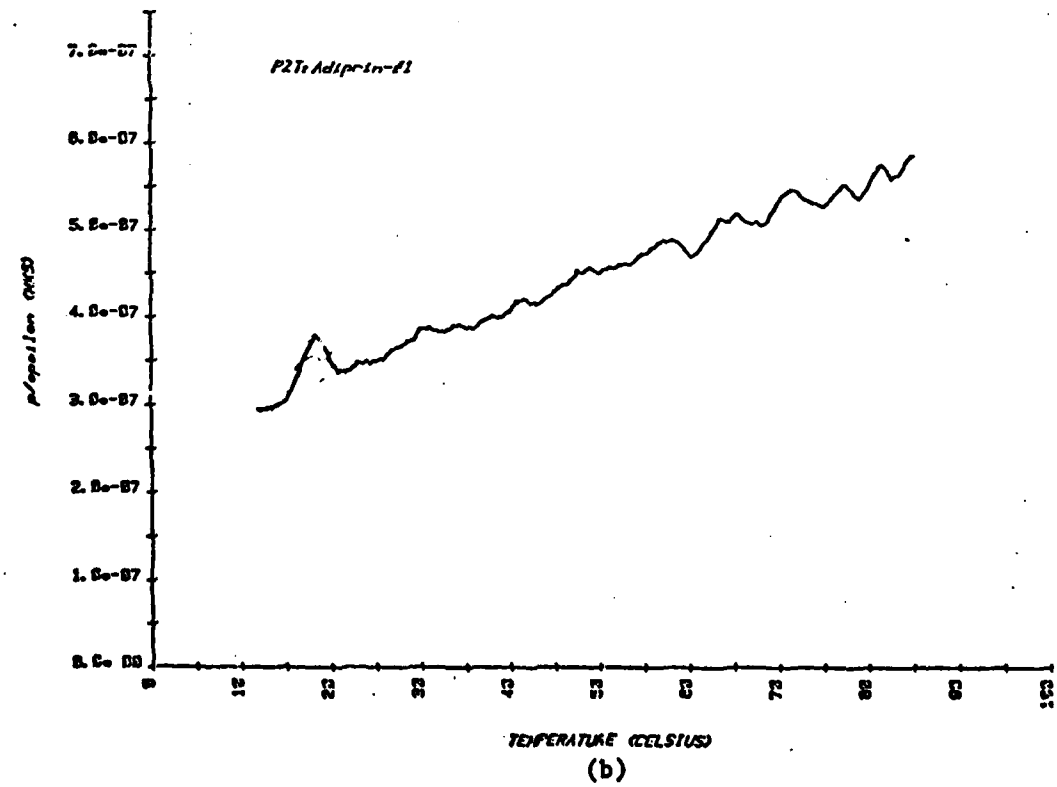

(b)

Figure 1. (a) pyroelectric coefficient and (b) Figure of merit p/ε of PZT:adiprin replamine composite of 6 mm thickness (absolute values of p).

shows a slight improvement over the PZT because of a greater reduction of ε compared to p.

(b) PZT:Spurrs Replamine. The pyroelectric behavior of two replamine PZT:Spurrs composites was measured. The first sample (3 mm thick) showed unusual pyroelectric behavior. As shown in Fig. 2, the sign of the pyroelectric reverses at 45°C. The reversal of $\bar{p}$ was a reproducible effect over ten temperature cycles. The dielectric constant was reduced from the PZT value, as expected for the replamine composite, producing an improved figure of merit $\bar{p}/\bar{\varepsilon}$ for temperatures well above or well below 45°C. The improvement in $\bar{p}/\bar{\varepsilon}$ at T ≈ 100°C is nearly a factor of five.

A thinner 0.75 mm replamine sample of PZT:Spurrs was also measured. The pyroelectric data are shown in Fig. 3. In contrast to the previous data on the PZT:Spurrs composite #1, these data showed no reversal in the sign of $\bar{p}$ (down to -10°C) and the figure of merit ($\bar{p}/\bar{\varepsilon}$) was inferior to the pure PZT at room temperature.

The difference in the data could be produced in several ways including: (i) difference in the microstructure of the coral making up the samples; (ii) existence of a critical sample size with respect to the basic microstructural unit of the composite.

Comparison of the microstructures of the PZT:Spurrs samples shows no significant difference in the coral matrices. The basic microstructure unit in the two samples is 100-150 μm. The large microstructural unit suggests a critical dimension with respect to normal sample thicknesses. The sample showing a change in sign of $\bar{p}$ was 3 mm thick, whereas the sample without a crossover was 0.75 mm thick.

The 3 mm PZT:Spurrs sample was thinned to 2, 1, and then 0.5 mm. At each stage the microstructure was examined and a full set of pyroelectric data

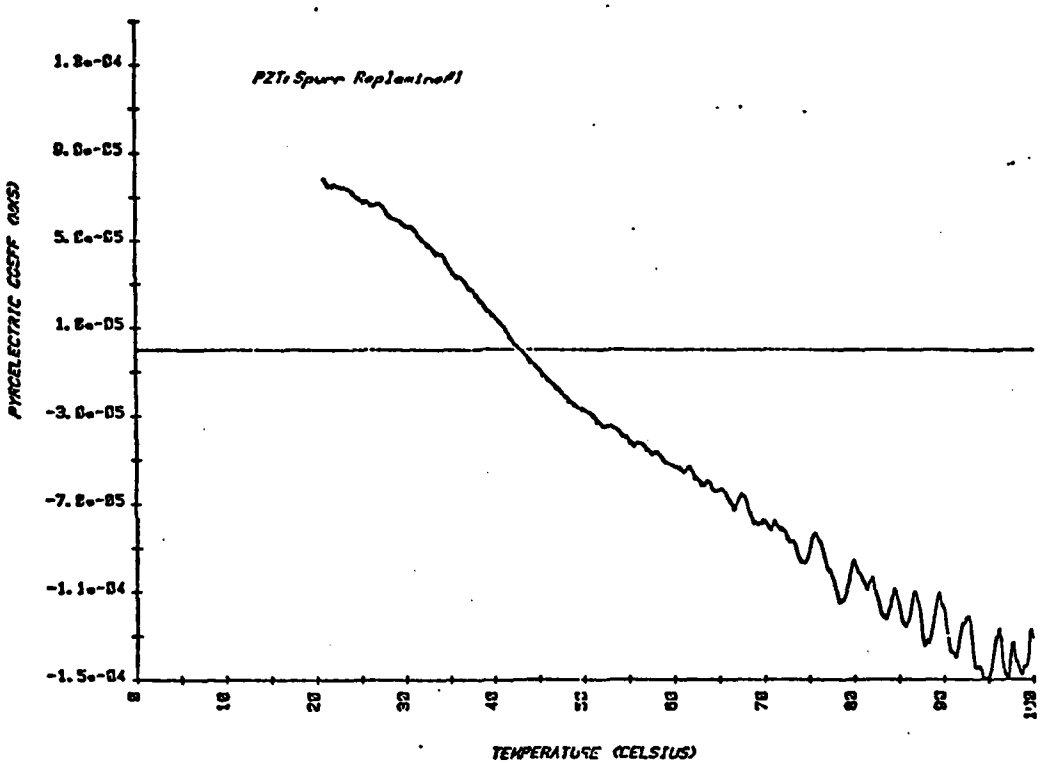

(a)

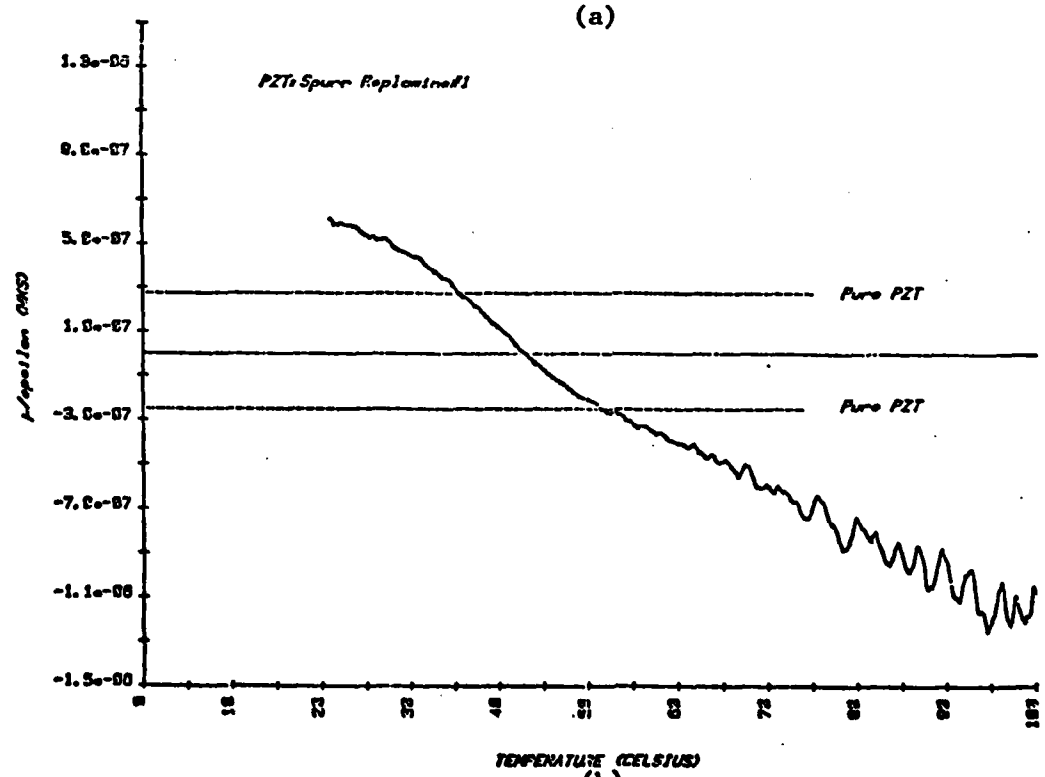

(b)

Figure 2. (a) Pyroelectric coefficient and (b) Figure of merit p/ε of PZT:spurs replamine composite; thickness 3mm. p/ε for the pure PZT is shown for comparison in (b).

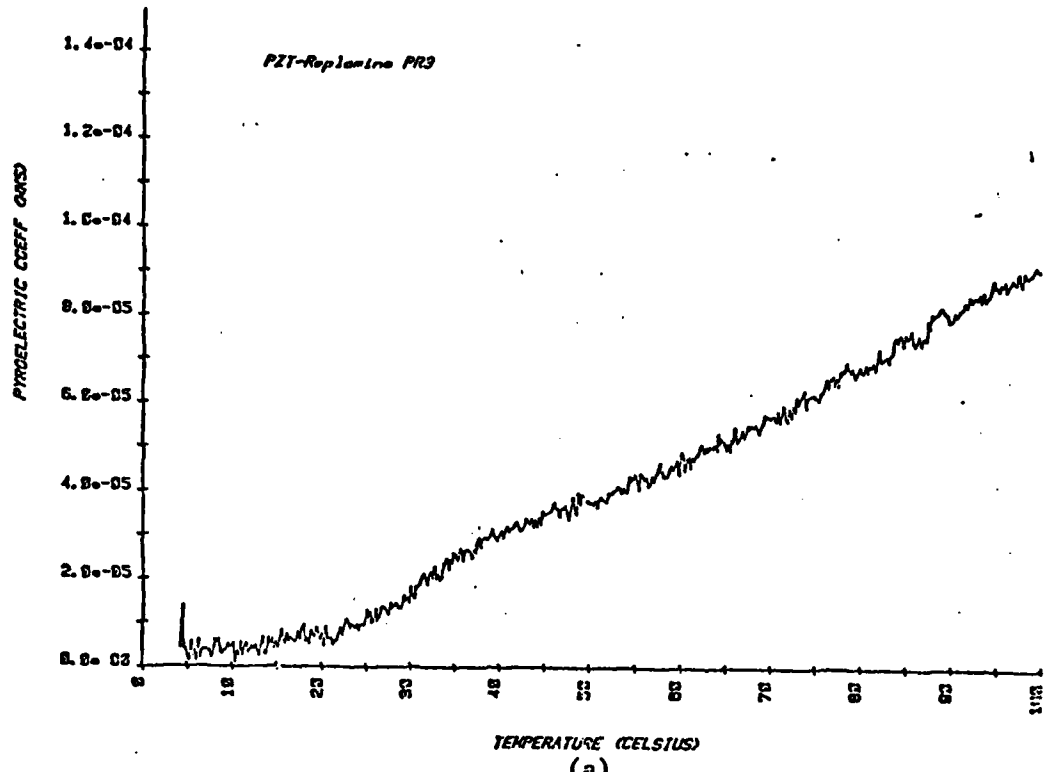

(a)

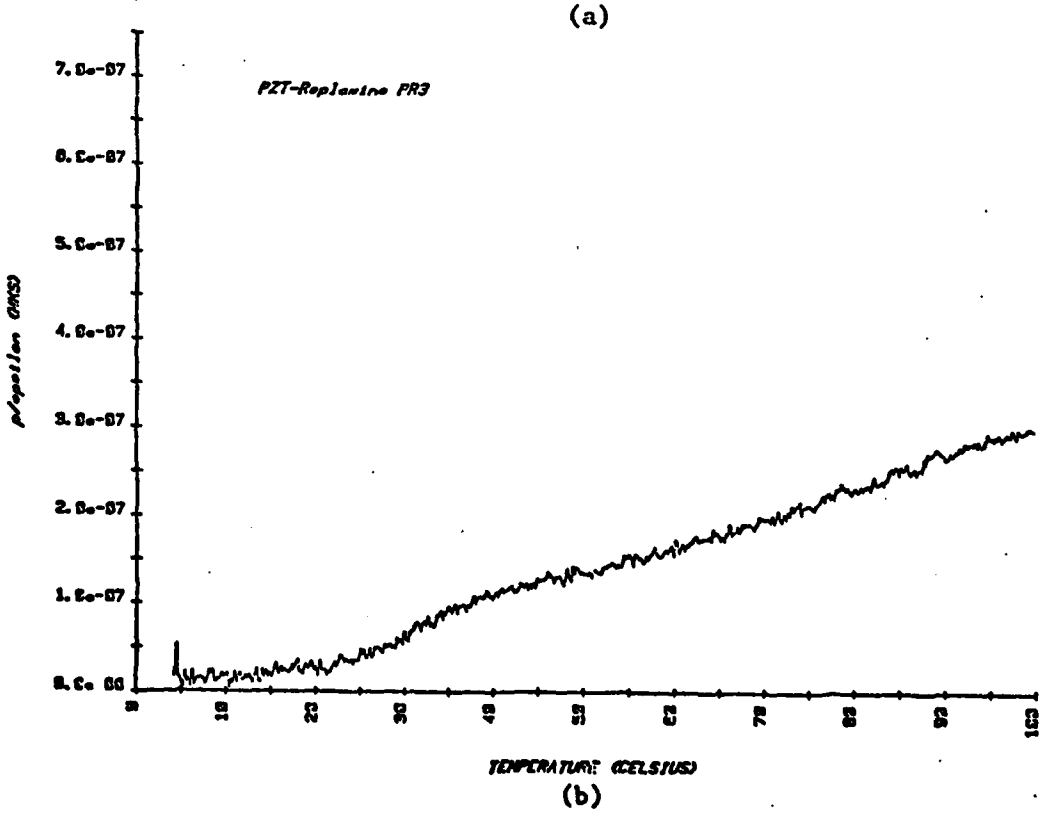

(b)

Figure 3. (a) Pyroelectric coefficient and (b) Figure of merit p/ε for a thin (0.7 mm) PZT:Spurrs replamine composite (absolute values of p).

measured. The microstructure was found to be homogeneous through the thickness. However, a thickness dependence in the pyroelectric behavior was observed as shown in Fig. 4. Data for the 3 mm thickness are not shown since the 2 mm data were essentially identical. While the details of the thickness behavior are not well understood, several important points emerge from the data:

1. Critical size effects show up for thicknesses as large as 6-10 microstructural units (the 1 mm sample).

2. For thicknesses of 3-5 microstructural units (the 0.5 mm sample), the qualitative behavior of p versus T differs from thicker samples.

3. For both regimes of thickness, samples show pyroelectric figures of merit ($\bar{p}/\bar{\epsilon}$) higher than the single phase material.

Measurements of $\bar{p}$, $\bar{\epsilon}$, $\bar{p}/\bar{\epsilon}$, and the comparative values of these composites to pure PZT are summarized in Table I. The pyroelectric response of the composites often show a sign reversal of the pyroelectric coefficient. Also, the magnitude of the pyroresponse decreases with the thickness at lower temperatures, but at high temperatures, the values for all the thicknesses are about the same. This behavior can be explained on the basis of equation [5] for the parallel connection model.

In the present composites the PZT and polymers are approximately in the 40% and 60% volume ratios. Taking the respective values of the constants for the two phases as

PZT		Polymer	
^1v	0·40	^2v	0·60
^1d	400 C/N	^2v	0
^1s	$18\times10^{-12}\ \frac{m}{N^2}$	^2s	$80\times10^{-12}\ \frac{m}{N^2}$
$^1\alpha$	10^{-6}/°C	$^2\alpha$	10^{-4}/°C

and substituting these numbers in the secondary contribution of equation [5],

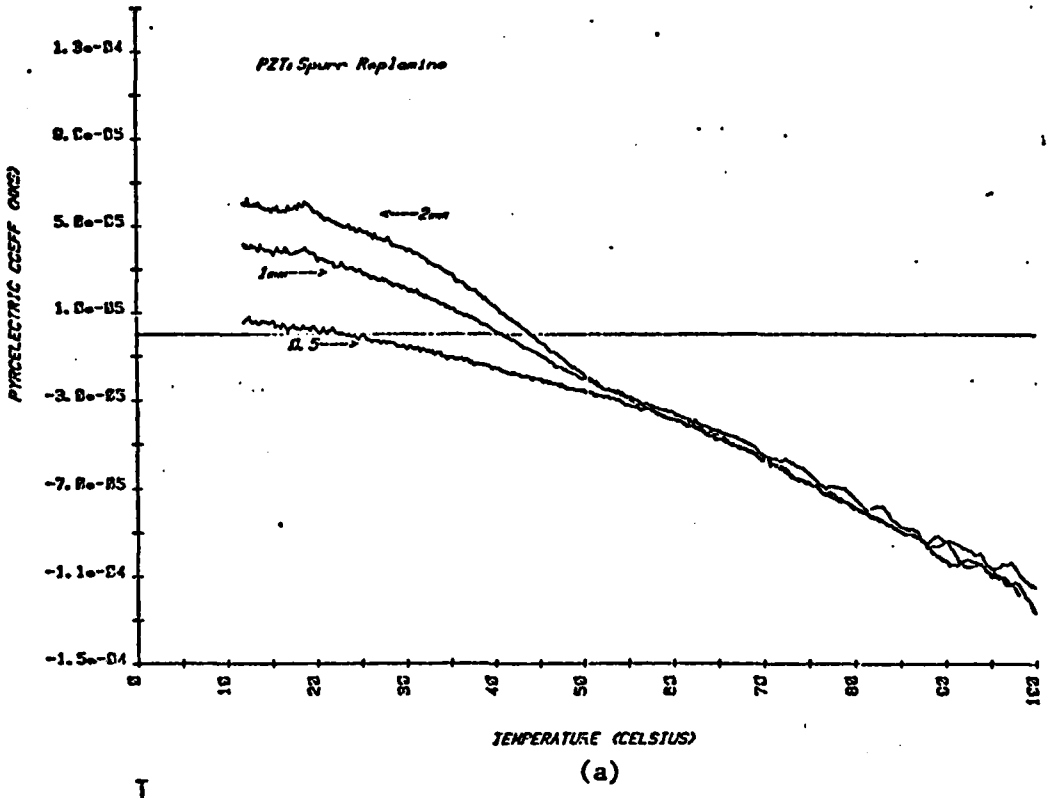

(a)

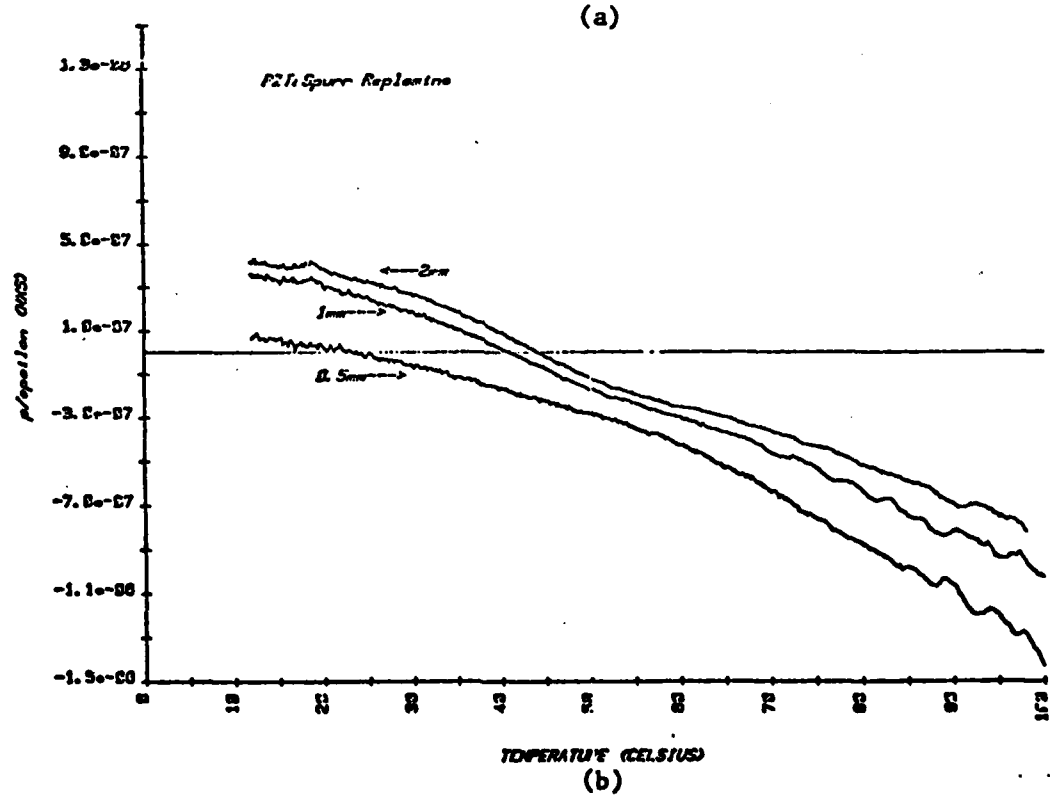

(b)

Figure 4. Thickness dependence (a); Pyroelectric coefficient & (b) figure of merit p/ε of PZT:Spurs replamine composite of 100-150 μm basic structural unit (Fig. 9).

Table I

Pyroelectric Figure of Merit of PZT Based Composites.

Sample	p $cm^{-2}{}^{\circ}K^{-1}$ ($\times 10^{-4}$)	ε_r	p/ε_r C $cm^{-2}{}^{\circ}K^{-1}$ ($\times 10^{-7}$)	$\frac{(\bar{p}/\bar{\varepsilon})}{(\bar{p}/\bar{\varepsilon})\ PZT}$ Comp
Pure PZT-501	5.0	1800	2.7 - 2.0	---
Loaded film	0.4	200	2.0	≈1.0
PZT:Adiprin	0.225	60	3.2	1.3
PZT:Spurrs (#1)	1.5	120	11.0	5.0 (100°C)
(3 mm thick)	0.8	130	6.0	2.2 (25°C)
PZT:Spurrs	0.9	300	3 (100°C)	1.5
(B-70,PR-3)	0.1	260	0.5 (20°C)	0.3
PZT:Spurrs (#1)				
2.0 mm thick	1.2	130	8	4.0
1.0 mm thick	1.2	100	11	5.5
0.5 mm thick	1.2	80	14	7.0

gives a value of $p_{sec} = +228\ \mu C/m^2{}^\circ C$. The total pyroelectric effect from composite at room temperature thus should be

$$p_T = {}^1v^1p + 228$$
$$= +28\ \mu C/m^2{}^\circ C.$$

The sign of the pyroelectric coefficient of the composite at room temperature is opposite to the total pyroelectric coefficient of pure PZT. At room temperature the polymer mechanically clamps the PZT, but at higher temperatures the polymer softens, reducing the clamping effect, and hence the secondary pyroelectric effect. At sufficiently high temperatures the secondary effect is very small, since the clamping is minimal and the major contribution is then from the primary part. This also suggests that the thickness effect should disappear at higher temperatures. This is clearly seen in Fig. 2. In this sample, the secondary effect almost cancels the primary effect and as the temperature rises the primary effect takes over. Also in case of the adiprin: PZT composite, clamping is very small, thus the secondary contribution is negligible and the pyroelectric response is essentially the primary part and the sample behaves as a dilute PZT system. Major changes were also noted when the sample thickness was comparable to the scale of the composite heterogeneity. Table I thus shows the enhanced $\bar{p}/\bar{\varepsilon}$ over the pure PZT by a factor of 5 on the dominant 3:1 connectivity samples.

There are also additional advantages of a composite target material. If a polymer is employed as the host material, the target would be stronger and more flexible than a ferroelectric single crystal. The thermal mismatch between the two phases of a composite pyroelectric could be altered by changing the reflectivity coefficient. Improvements in the density, specific heat and lateral thermal diffusivity are also expected.

Summary

It is demonstrated that

(i) In PZT:SPURRS composites fabricated by the replamine process in dominant 3:1 connectivity, the simple pyroelectric figure of merit $\bar{p}/\bar{\varepsilon}$ can be enhanced by a factor of 5 to 7.

(ii) The data support the original hypothesis that the mode of phase interconnection is critical to the mechanism of enhancement in that the PZT: Spurrs composites and PZT:soft polymer (adiprin) composites do not exhibit comparable properties.

(iii) The scale of microstructure vs. the smallest sample dimension can make a major change in the response.

References

1. Singer, B., "Advances in Image Pick up and Display," Edited by B. Kagan, Academic Press, NY (1977).
2. Newnham, R. E., Skinner, D. P., and Cross, L. E., Mat. Res. Bull. 13, 525 (1978).
3. Skinner, D. P., Newnham, R. E., and Cross, L. E., Mat. Res. Bull. 13, 599 (1978).
4. Bhalla, A. S., and Newnham, R. E., Physica Stat. Solidi (a) (to be published).
5. Chynoweth, A. G., Phys. Rev. 102, 705 (1956).
6. Byer, R. L., and Roudy, C. B., Ferroelectrics 3, 333 (1972).

APPENDIX I

Primary and Secondary Pyroelectricity

A.S. Bhalla and R.E. Newnham

Primary and Secondary Pyroelectricity

by

A.S. Bhalla and R.E. Newnham
Materials Research Laboratory
The Pennsylvania State University
University Park, PA 16802 USA

The pyroelectric coefficient (p) of a material under constant stress and electric field is defined by the expression

$$p = \left(\frac{\partial P_s}{\partial T}\right)_{E,\sigma} \qquad (1)$$

where P_s is the spontaneous polarization, T the temperature, E the electric field and σ the elastic stress[1,2]. Thermodynamic analysis of the pyroelectric effect yield the expression

$$p_i^{\sigma} = p_i^{\varepsilon} + d_{ijk}^{T}\, c_{jklm}^{T,E}\, \alpha_{lm}^{\sigma} \qquad (2)$$

where P_i^{σ} is the total pyroelectric effect measured at constant stress, and P_i^{ε}, the pyroelectric effect at constant strain ε, is called the primary effect. The second term of equation (2) is the contribution caused by thermal deformation of the crystal and is known as the secondary pyroelectric effect. d, c and α are the piezoelectric, elastic stiffness and the thermal expansion coefficients of the crystal, respectively. (A third contribution to the pyroelectric effect, known as the tertiary pyroelectric effect[3], arises from inhomogeneous temperature distributions within the sample. Since the origin of the tertiary effect depends on experimental conditions, it is not included in the present study).

In ferroelectric pyroelectrics the primary effect is large and negative because the spontaneous polarization diminishes with increasing temperature. The secondary effect is considerably smaller and may have either sign depending on the values of the constants. Thus the experimentally observed pyroelectric coefficients are dominated by the primary effect and are negative in ferroelectric crystals. In non-ferroelectric pyroelectric crystals there is no simple way to predict the sign and the magnitude of these coefficients. In practice the total pyroelectric effect can be measured and secondary effect calculated from the constants d, α and c. But in only a few materials[4] have the primary and secondary pyroelectric components been evaluated: $BaTiO_3$ [5], PZT [6,7], $Li_2SO_4.H_2O$ [8] and $Sr_{0.5}Ba_{0.5}Nb_2O_6$ [9].

For a number of applications, such as infrared detectors and vidicons, it is desirable to know the magnitude and sign of the contributions to the total pyroelectric effect. During our studies of diphasic pyroelectric composites[10], we surveyed various families of pyroelectric materials and separated the primary and the secondary effects. The results are listed in Table 1. The secondary contributions for various crystal symmetry groups were calculated from the following equations.

$$p_{sec} = d_{21}(c_{11}\alpha_1+c_{12}\alpha_2+c_{13}\alpha_3+c_{15}\alpha_5) + d_{22}(c_{12}\alpha_1+c_{22}\alpha_2+c_{23}\alpha_3+c_{25}\alpha_5) + d_{23}(c_{13}\alpha_1+c_{23}\alpha_2+c_{33}\alpha_3+c_{35}\alpha_5) + d_{25}(c_{15}\alpha_1+c_{25}\alpha_2+c_{35}\alpha_3+c_{55}\alpha_5)$$

Point group 2

b polar axis

$$p_{sec} = d_{31}(c_{11}\alpha_1+c_{12}\alpha_2+c_{13}\alpha_3) + d_{32}(c_{12}\alpha_1+c_{22}\alpha_2+c_{23}\alpha_3) + d_{33}(c_{13}\alpha_1+c_{23}\alpha_2+c_{33}\alpha_3)$$

Point group mm2

c polar axis

$$p_{sec} = 2d_{31}(c_{11}\alpha_1+c_{12}\alpha_1+c_{13}\alpha_3) + d_{33}(2c_{13}\alpha_1+c_{33}\alpha_3)$$

Point groups 3,3m,4,4mm,6,6mm

c polar axis

Point group ∞mm of the poled ceramic samples leads to equations equivalent in form to the hexagonal crystal system. The ∞ axis is parallel to the poling direction and is denoted as x_3.

The values of the constants are taken from the recent literature or from the Landolt-Bornstein Tables, as noted in Table 1. It is evident from the data that in ferroelectric ceramics and single crystals, both the primary and total pyroelectric effects are large and negative. Secondary coefficients in ferroelectric single crystals are comparatively small and positive with the exception of SBN and $NaNO_2$ where the secondary pyroelectric effect is small and negative, enhancing the primary pyroelectric effect. In TGS, $Ba_2NaNb_2O_5$ and the ceramics PZT and $BaTiO_3$, the secondary effect is more substantical.

Compared to ferroelectris, tourmaline and other nonferroelectric

polar materials show rather small pyroelectric effects. In these materials, the total and the secondary coefficients carry the same sign, and in most cases they are positive. The secondary effect arising from piezoelectricity and thermal expansion makes a large contribution to the total pyroelectric effect. In tourmaline for instance, 80% of the pyroelectric signal is of secondary origin. Fresnoite, $Ba_2TiSi_2O_8$, is another mineral in which pyroelectricity is dominated by the secondary effect. In semiconductor pyroelectrics with the wurtzite structure, the effect is very small, with all coefficients having the same sign.

It is clear from the table that both the primary and secondary effects are important, and that certain trends emerge regarding the magnitude and sign of the coefficients. All pyroelectric materials do not follow the same pattern, but members of the same family share common features: in ferroelectrics all the observed coefficients are negative and dominated by the primary effect, in contrast to non-ferroelectric pyroelectrics where secondary effects are more substantial.

Acknowledgments

This work was sponsored by the Office of Naval Research through contract N00014-78-C-0291 and Advanced Research Project Agency through contract MDA 903-78-C-0306.

References

1. J.F. Nye "Physical properties of Crystals" Oxford University Press. London 1957, p.189.
2. R.E. Newnham "Structure - Property Relations" Springer-Verlag, New York (1975).
3. L.B. Schein, P.J. Cressman and L.E. Cross. Ferroelectrics 22, 945 (1979).
4. Ferro and Antiferroelectric materials Vol. III/3/ (1973), Vol. III/V (1975), and Numerical Data and Functional Relationships in Science and Technology Vol. 11 (1978), edited by H. Hellwege (Landolt-Bornstein, New Series).
5. T.A. Perls, T.J. Diesel and W.I. Bobrov. J. Appl. Phys. 29, 1297 (1958).
6. W.R. Cook, Jr., D.A. Berlincourt and F.J. Scholz. J. Appl. Phys. 34, 1392 (1963).
7. L.Z. Kennedy and J.L. Wentz. J. Appl. Phys. 35, 1767 (1964).
8. S.B. Lang. Phys. Rev. B4, 3603 (1971).
9. S.T. Liu and L.E. Cross. Phys. Stat. Sol. (a) 41, K83 (1977).
10. R.E. Newnham, D.P. Skinner, K.A. Klicker, A.S. Bhalla, B. Hardiman and T.R. Gururaja (under publication) Ferroelectrics.

11a. S. Haussühl and J. Albers. Ferroelectrics. 15, 73 (1977).

11b. T. Ikeda, Y. Tanaka and H. Toyoda. Jap. J. Appl. Phys. 1, 13 (1962).

12. R.L. Byer and C.R. Roundy. Ferroelectrics. 3, 333 (1972).
13. A.M. Glass and M.E. Lines. Phys. Rev. B13, 180 (1976).
14. A.W. Warner, M. Onoe and G.A. Coquin. J. Acoust. Soc. Am. 42, 1223 (1967).
15. T. Yamada, H. Iwasaki and N. Nizeki. J. Appl. Phys. 43, 772 (1972).
16. G.R. Jones, N. Shaw and A.W. Vere. Electron. Letters 8, 345 (1972).
17. A.W. Warner, G.A. Coquin and J.L. Fink. J. Appl. Phys. 40, 4353 (1969).
18. S. Singh. S.A. Dracger and J.G. Geusic. Phys. Rev. B2, 2709 (1970).
19. R.B. Rice and H. Fay. J. Appl. Phys. 40, 909 (1969).
20. S. Hoshino and I. Shibuya. J. Phys. Soc. (Japan). 16, 1254 (1961).
21. B.G.F. Taylor and H.A.H. Boot. Contemp. Phys. 14, 55 (1973).
22. S.B. Lang. Nature. 224, 798 (1969).

23a. S. Haussühl. J. Cryst. Growth. 40, 200 (1977).

23b. M. Kimura. Jap. J. Appl. Phys. 48, 2850 (1977).

24. D.S. Robertson, I.M. Young, F.W. Ainger, C. O'Hara and A.M. Glazer. J. Phys. D:Appl. Phys. 12, 611 (1979).
25. V.V. Gladkii and I.S. Zheludev. J. Phys. Crystallography. 12, 788 (1968).
26. D. Berlincourt, H. Jaffe and L.R. Shiozawa. Phys. Rev. 129, 1009 (1963).

27. T.B. Bateman. J. Appl. Phys. 33, 3309 (1962).

28. G. Heiland and H. Ibach. Sol. State Commun. 4, 353 (1966).

29. Thermophysical Properties of Matter. (The TPRC data service) Vol. 13, Thermal Expansion - Non metallic Solids.

TABLE 1

Primary, secondary and the observed pyroelectric effect in various pyroelectric materials. Room-temperature values.

Materials	Point group symmetry	Observed total effect $\mu C/m^2{}^\circ K$	Calculated secondary effect $\mu C/m^2{}^\circ K$	Primary effect $\mu C/m^2{}^\circ K$	References
A) Ferroelectrics					
a) Ceramics					
$Pb(Zr_{0.52}Ti_{0.48})O_3$:1wt%$Nb_2O_5$	∞mm	- 50	+60	-110.0	[6]
$BaTiO_3$	∞mm	-190.0	+80.0	-270.0	[5]
$Pb(Zr_{0.95}Ti_{0.05})O_3$:1wt%$Nb_2O_5$	∞mm	-268.0	+37.7	-305.7	[7]
b) Single Crystal					
$Sr_{0.5}Ba_{0.5}Nb_2O_6$	4mm	-550	-21.0	-529.0	[9]
TGS	2	-270	+60.0	-330.0	[11], [12]*
$LiTaO_3$	3m	-176	+ 2.00	-178	[4], [12]
$LiNbO_3$	3m	- 83.0	+12.9	- 95.9	[4], [14], [13]
$Pb_5Ge_3O_{11}$	3	- 95.0	+15.5	-110.5	[4], [15], [16]
$Ba_2NaNb_5O_{15}$**	2mm	-100.0	+41.8	-141.8	[17], [18], [19]
$NaNO_2$	2mm	-140.0	- 5.0	-135.0	[20], [4], [21]
B) Non Ferroelectric					
$Li_2SO_4.H_2O$	2	+ 86.3	+26.1	+ 60.2	[8]
Tourmaline	3m	+ 4.0	+ 3.2	+ 0.8	[1]
Bone	∞	$+25\times10^{-4}$	$+117\times10^{-4}$	-92.0×10^{-4}	[22]
$Ba_2Si_2TiO_8$	4mm	+10	+22, +16	- 12.0, - 6.0	[23]
Li_2GeO_3	2mm	-27	-12.8	- 14.2	[24]
$Ba(NO_2)_2.H_2O$		- 25.3	- 3.3	- 22.0	[25]

TABLE 1 (Cont'd)

Primary, secondary and the observed pyroelectric effect in various pyroelectric materials. Room-temperature values.

Materials	Point group symmetry	Observed total effect $\mu C/m^2 °K$	Calculated secondary effect $\mu C/m^2 °K$	Primary effect $\mu C/m^2 °K$	References
C) Semiconductor					
CdS	6mm	-4.0	-1.0	-3.0	[26]
CdSe	6mm	-3.5	-0.56	-2.94	[26]
ZnO	6mm	-9.4	-2.5	-6.9	[27], [28]
ZnS***	6mm	0.43	+0.34		[4], [29]
BeO	6mm	-3.40	-0.008	-3.39	[4], [29]

* average value of the wide range of reported values between 200-350 $\mu C/m^2 °K$.

** maximum value of p measured on the sample.

*** no reported sign for p_i^{σ}; no information about polytypic nature of the sample.

APPENDIX II

PYROELECTRICITY IN SbSI

PYROELECTRICITY IN SbSI

Antimony sulfur iodide (SbSI) is the most important member of a family[1,2] of ferroelectric conductors with formula $A^{V}B^{VI}X^{VII}$. It has a displacive first order ferroelectric transition near 20°C. The Curie temperature T_c depends on the growth method and chemical stoichiometry of the crystal[3,4]. In the ferroelectric phase, SbSI belongs to point group mm2 in the orthorhombic system and exhibits a very large structural anisotropy along the polar c-axis[5,6]. The transition is accompanied by an exceedingly high permittivity at T_c. Crystals grow as bundles of fine needles parallel to the c-axis. It is rather difficult to make good electrical measurements on these crystals because of their small cross-sectional area and the uncertainty of the single-crystal nature of the sample. So far, no reliable measurements of the pyroelectric coefficient and its temperature dependence have been reported in the literature. In this paper we describe measurements of the pyroelectric and dielectric constants[7] on SbSI crystals using the Byre-Roundy method[8]. This technique eliminates uncertainties in temperature by measuring p and ε simultaneously. The pyroelectric figure of merit p/ε is evaluated over a temperature range encompassing the ferroelectric phase transition.

Measurement Technique

Measurements of the pyroelectric coefficient p and the dielectric permittivity ε for samples were carried out using an automated measurement technique[7]. In this system, the pyroelectric coefficient is determined by measuring the DC discharging (or charging) current (i) from a sample of known electrode area (A) subjected to a controlled rate of change of temperature (dT/dt). The pyroelectric coefficient p is given by

$$p = \frac{i/A}{dT/dt} \qquad (1)$$

It is important to compare the measured pyroelectric coefficient for both heating and cooling over a number of temperature cycles because there are several possible sources of current arising from the release of trapped or injected charge and from conduction currents under bias. Comparing heating and cooling curves after different modes of poling and under different cycling conditions provides a way of separating some of these extraneous effects.

Simultaneous pyroelectric and dielectric measurements are made by dividing the circuit into high and low frequency parts. The low frequency (essentially DC) side of the circuit is used to apply the DC bias and measure the capacitance at 1 MHz through the high frequency branch of the circuit. The two halves are electrically isolated from each other. Automated control is accomplished with a Hewlett-Packard 3052A Automated Data Acquisition System. The pyroelectric measurement system is based on a HP9825A minicomputer with instrument control and data transfer provided by the HPIB interface bus (IEEE 488 Standard). Data are stored on magnetic tape cartridges and plotted on a digital plotter. The computer controls the temperature (heating rate) and bias applied to the sample. The overall system speed is 3 to 4 complete measurement cycles per second with data stored only when any one of the measured quantities exceeds a preset percentage of absolute charge.

The sample temperature is determined with the well-calibrated platinum resistance thermometer. Time is determined using the HP98035A interface clock. From the time and temperature measurements, dT/dt is calculated. In our arrangement, the pyroelectric coefficient can be studied in the temperature range between -30 and 200°C.

Experimental

Crystals of SbSI were grown from an SbI_3 flux using the Bridgman method and the vapor transport technique[9,10]. A few good quality single crystals

with well-defined morphology were selected. Crystals were checked under an optical microscope for optical quality and possible inclusions. Chemical homogeneity was evaluated by electron microprobe analysis in a scanning electron microscope. Vapor-grown crystals were slightly off stoichiometry with a slight excess of sulfur together with oxygen impurities. Cross-sectional areas of the crystals were measured by optical microscopy. Two ends of the crystals were electroded with Ag-paste and gold wires 5 mil in diameter were attached to the end. Crystals were suspended from the gold wire electrodes in a special specimen holder and then placed in a silicone oil bath. The SbSI samples were kept dark to avoid the possibility of photocurrents. Samples were poled with DC fields of 500 V/cm to 1 KV/cm while being cooled from 45°C to about 10°C. At 10°C the poling field was removed gradually in order to minimize the possibility of back switching caused by the space charge built up under DC field. Samples were held at that temperature up to several hours before collecting the pyroelectric data in the heating cycles. Typical heating rates were 1°C/min to 4°C/min in various runs.

Results and Discussion

Figure 1 shows the temperature dependence of the dielectric constant of vapor-grown SbSI measured at 1 MHz with and without extra bias. An electric field of -500 V/cm was applied while heating the crystal in Run No. 1 and during the cooling cycle in Run No. 2. In Run No. 3 the sample was heated at 2°C/min from 5°C to 40°C under zero field. Simultaneous measurements of the sample capacitance and the pyroelectric output current were made. The sample was then cooled through the phase transition under a positive field of 500 V/cm. Dielectric and pyroelectric data were again collected in Run No. 5 while heating the sample.

Figure 2 shows the current density measured during cycles No. 3 and 5. The change in sign of the current density with the reversal of the poling field

indicates clearly that the origin of the current is the pyroelectric effect in SbSI. The pyroelectric coefficients calculated from equation 1 are plotted in Figure 3 for various temperatures. The pyroelectric coefficients are unusually large, even at temperatures well removed from the transition (Figure 4). In the vapor-grown crystals, typical values of the pyroelectric coefficients were 1.2×10^4 $\mu c/m^2 °K$ at $(T-T_c) = 2°$ and 6×10^4 $\mu c/m^2 °K$ at the peak respectively. The spontaneous polarization (P_s) 23 $\mu c/cm^2$ (Figure 5) calculated from the integration of pyroelectric current agrees well with the value of 25 $\mu c/cm^2$ reported in the literature.

Both the dielectric and the pyroelectric data show a sharp transition around 24.7°C, slightly higher than the value reported for flux-grown crystals. Apparently the vapor-grown crystals contain oxygen impurities and excess sulfur which result in a small increase in the transition temperature. The pyroelectric properties are apparently not affected by the impurities, as evident from the pyroelectric data gathered on flux-grown crystals.

The pyroelectric figure of merit (p/K) for SbSI was computed from the pyroelectric coefficient p and the dielectric constant K measured at various temperatures, and is plotted in Figure 6. From 5°C to about 20°C, p/K is 2×10^{-6} (MKS) but rises sharply to 10^{-5} at the transition.

According to Devonshire's phenomenological theory of ferroelectricity, for a crystal in the stress-free state thermodynamic potential A(P) can be expressed as

$$A(P) = A_0(T) + \frac{\beta}{2}(T-T_0)P^2 + \frac{rp^4}{4} + \frac{\delta p^6}{6} + \ldots \qquad (2)$$

where p is the electric polarization and β, r, and δ are temperature-

independent coefficients. Using only the second order forms, Liu and Zook[11] derived a relation

$$\frac{p}{K} = \frac{P_s}{c} \tag{3}$$

where c is the curie constant and assumed to be temperature independent. The equation (3) dictates that the figure of merit p/K should follow the slope of P_s vs T curve. The validity of this relation was tested on SBN using an automated Byre-Roundy technique[12]. The experimental values and the theoretical predictions are in agreement over a temperature range 20°C below the transition in TGS and DTGFB.

It is clear from Figures 5 and 6 that p/K(T) does not follow the temperature dependence of P_s. The discrepancy might be real, or it could arise from errors in the measured values of p and K. The spontaneous polarization P_s computed from the integration of p is in good agreement with the value obtained from the E-D curve supporting the validity of the pyroelectric coefficient measurements. This suggests the possibility of discrepancies in the dielectric constant. In the present set-up the dielectric constants at 1 MHz are not measured under steady-state conditions, and thus do not give the isothermal values needed to establish the validity of relation (3). The measured values are closer to the adiabatic dielectric permittivity. This suggests a correction to the measured permittivity based on the following relation[13].

$$K_T = K_s + \frac{p^2 T}{\epsilon_o c_p} \tag{4}$$

where K_T and K_s are the isothermal and adiabatic dielectric constants, and the volume specific heat of SbSI. Isothermal dielectric constants were calculated at various temperatures and plotted in Figure 7. A sharp dielectric anomaly representing the first order transition appears at 24.7°C. Revised plots of (p/K_T) vs T and (P_s/c) vs T are shown in Figure 8. Both functions have a

sharp decrease near the curie temperature, but some anomalies in p/K_T remain. Further study of the higher order terms in the Devonshire theory and of the temperature dependence of the property coefficients is needed.

The highest value of the figure of merit (p/K_T) is about 2.4×10^{-6} measured 5° below T_c.

References

1. Fatuzzo, E., Harbeke G., Merz, W.J., Nitsche, R., Roetchi, H. and Ruppel, W. Phys. Rev. 127, 2036 (1962).
2. Nitsche, R. and Merz, W.J. J. Phys. Chem. Solids 13, 154 (1960).
3. Belyaev, L.M., Lyakhovitskaya, V.A. and Sil'vestrova, I.M. Izv. Akad. Nauk SSSR, Neorgan. Mat. 6, 429 (1970).
4. Boksha, S.S., Lyakhovitskaya, V.A., Sil'vestrova, I.M. and Tikhomirova, N.A. Izv. Akad. Nauk SSSR Neorgan. Mat. 6, 1951 (1970).
5. Dönges, E. Z. anorg. allgem. Chem. 263, 112 (1950).
6. Kikuchi, A., Oka, Y. and Sawaguchi, E. J. Phys. Soc. (Japan) 23, 337 (1967).
7. Dougherty, J.P. and Seymour, R.J. Rev. Sci. Inst. (to be published).
8. Byre, R.L. and Roundy, C.B. Ferroelectrics 3, 333 (1972).
9. Bhalla, A.S., Spear, K.E. and Cross, L.E. Mat. Res. Bull. 14, 423 (1979).
10. Nassau, K., Shiever, J.W. and Kowalchik, M. J. Cryst. Growth 7, 237 (1970).
11. Liu, S.T. and Zook, J.D. Ferroelectrics 7, 171 (1974).
12. Seymour, R.J., Dougherty, J.P. and Shaulov, A. Phys. Rev. Letters (submitted).
13. Lines, M.E. and Glass, A.M. Principles and Applications of Ferroelectrics and Related Materials, Clarendon Press, Oxford, 1977, p. 129.

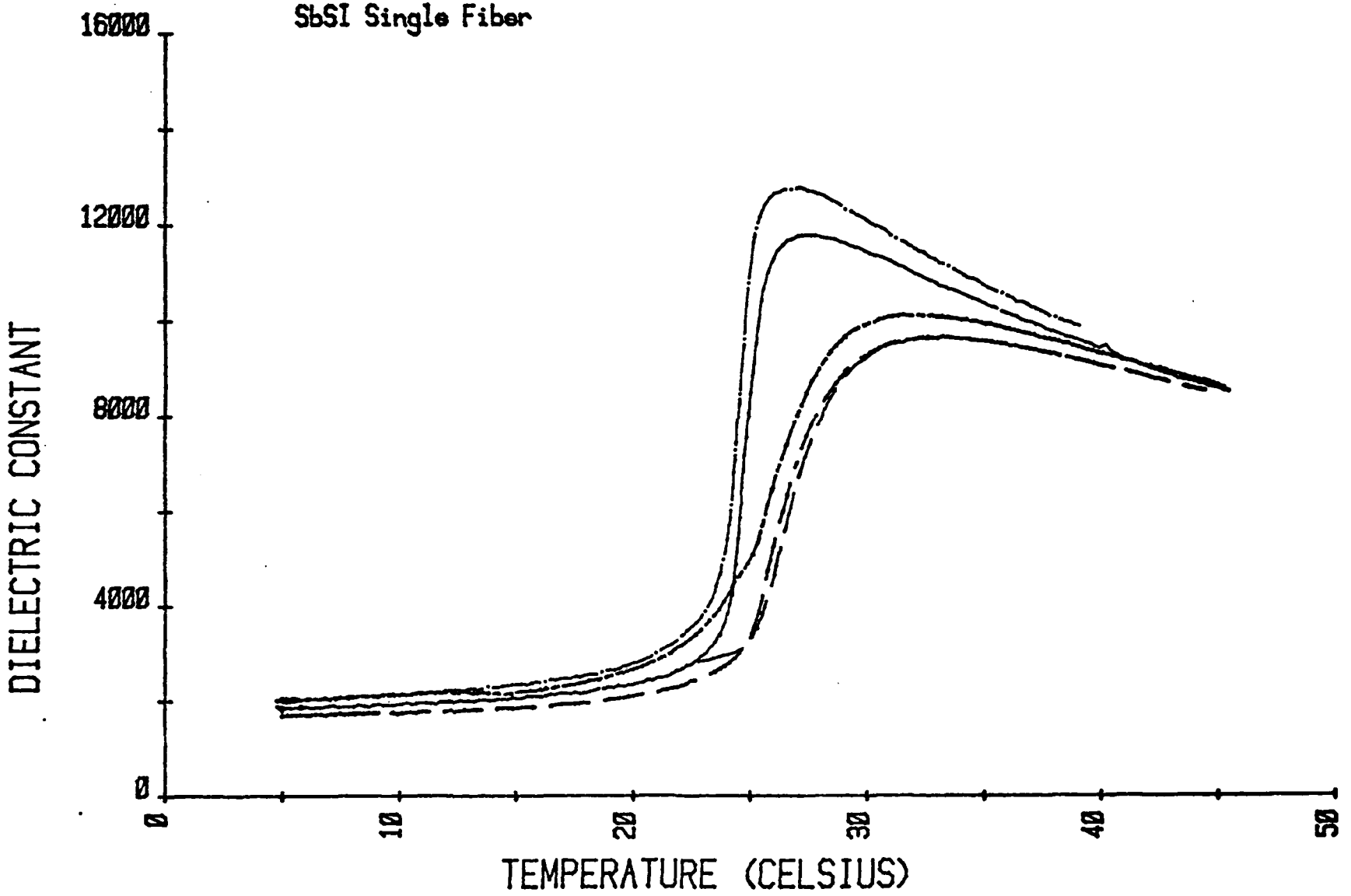
SbSI Single Fiber
16000
12000
8000
4000
0
DIELECTRIC CONSTANT
0
10
20
30
40
50
TEMPERATURE (CELSIUS)

Figure 1

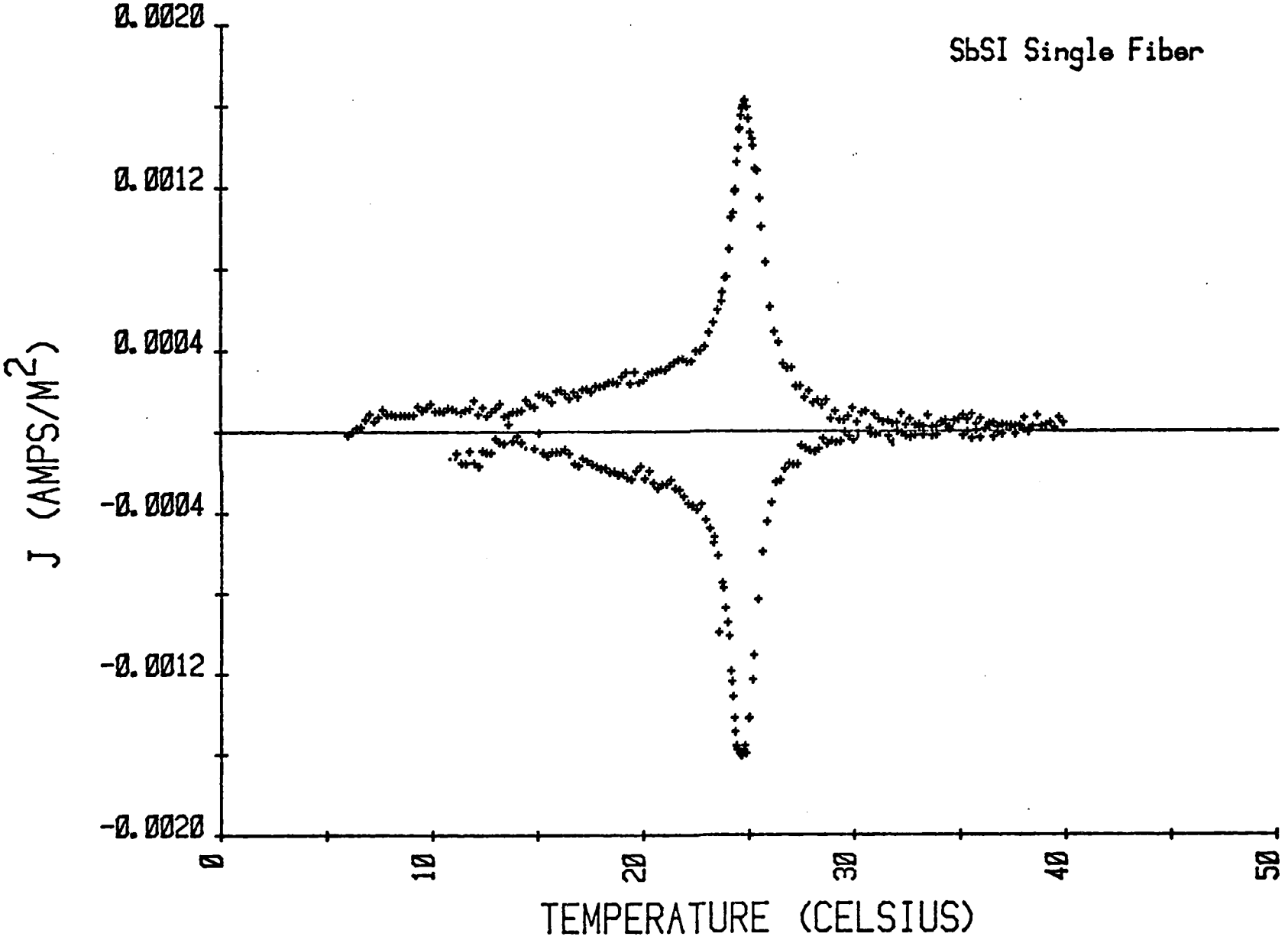
SbSI Single Fiber
0.0020
0.0012
0.0004
-0.0004
-0.0012
-0.0020
J (AMPS/M2)
0
10
20
30
40
50
TEMPERATURE (CELSIUS)

Figure 2

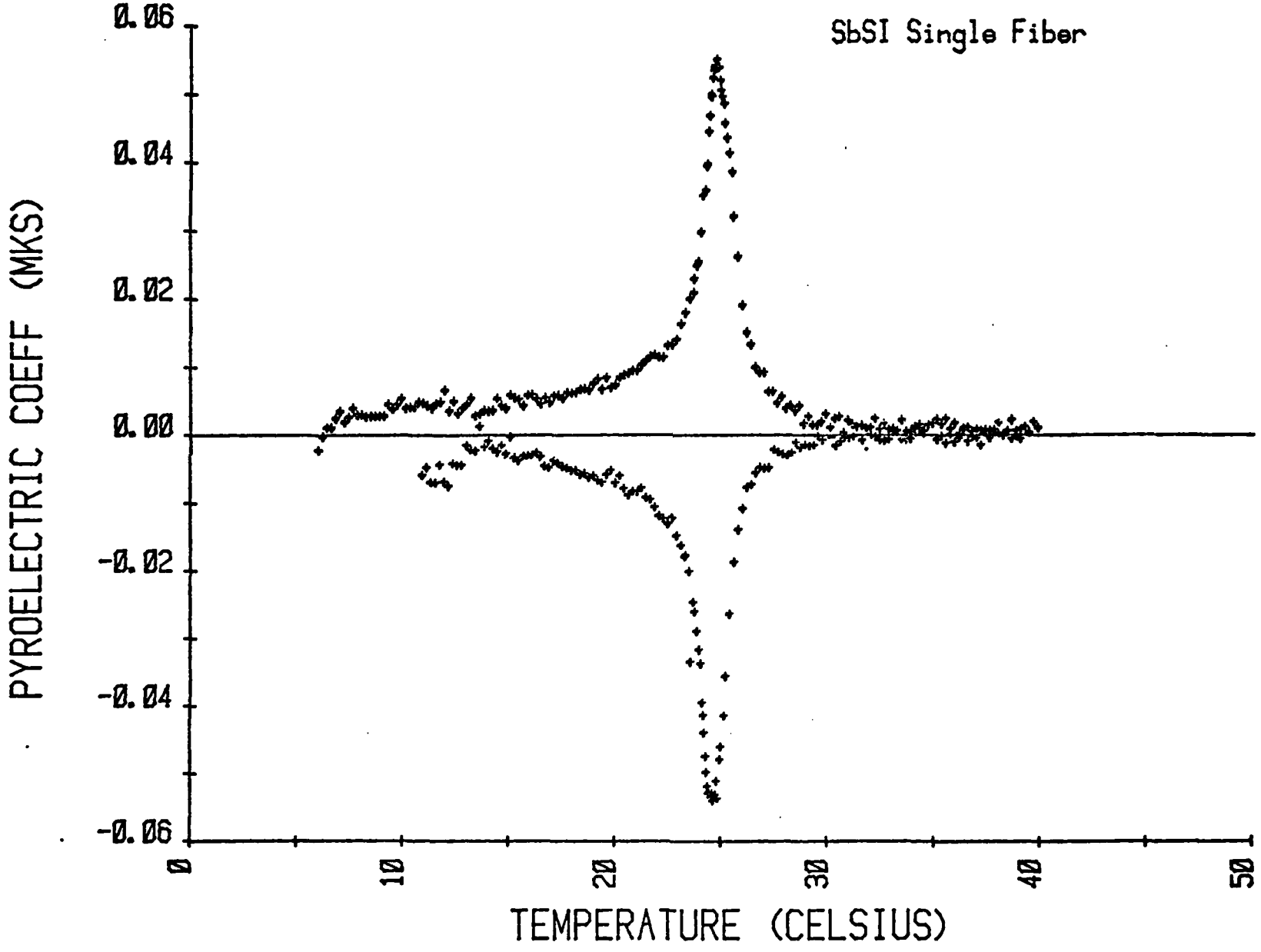
SbSI Single Fiber
PYROELECTRIC COEFF (MKS)
0.06
0.04
0.02
0.00
-0.02
-0.04
-0.06
0
10
20
30
40
50
TEMPERATURE (CELSIUS)

Figure 3

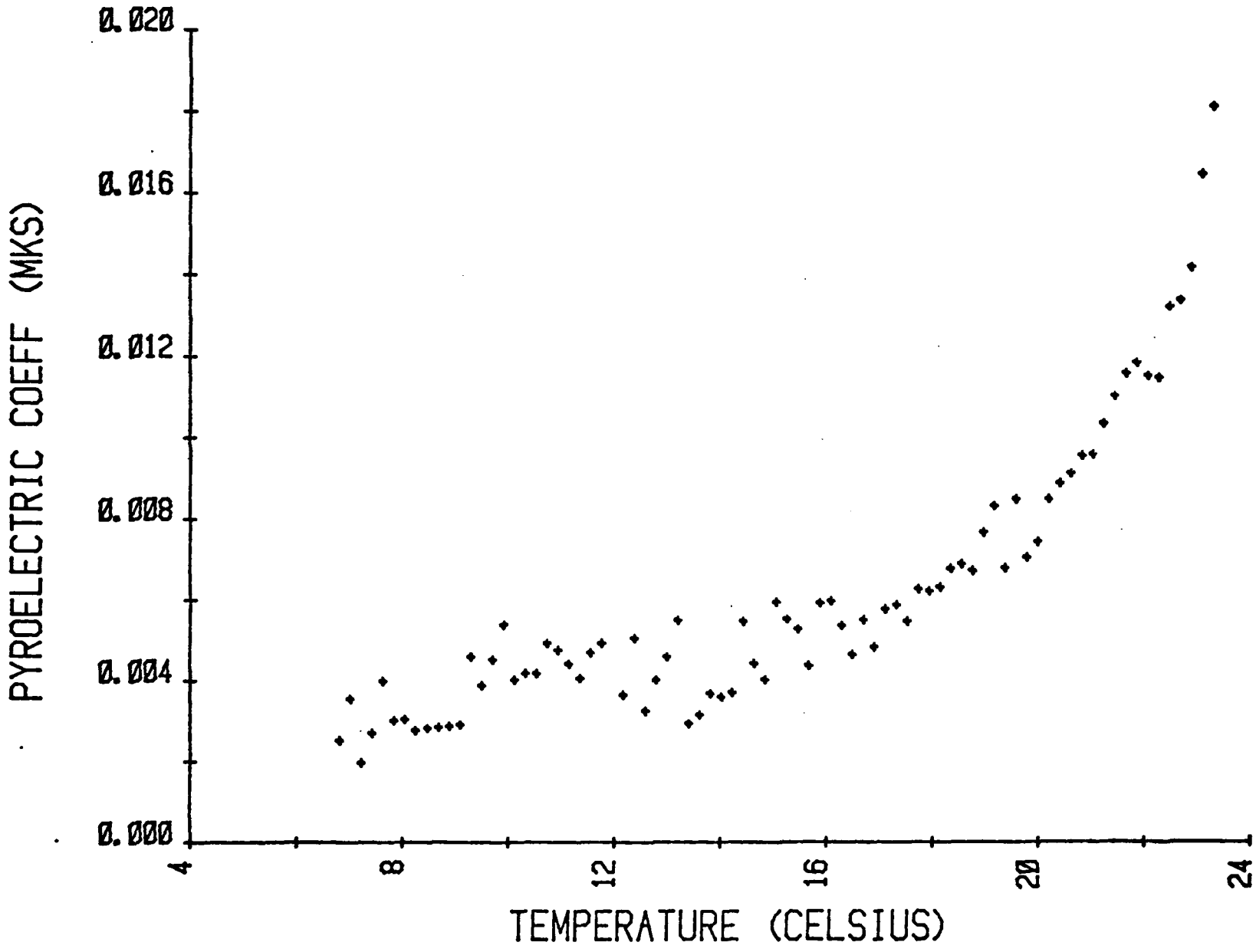
0.020
0.016
0.012
0.008
0.004
0.000
PYROELECTRIC COEFF (MKS)
4
8
12
16
20
24
TEMPERATURE (CELSIUS)

Figure 4

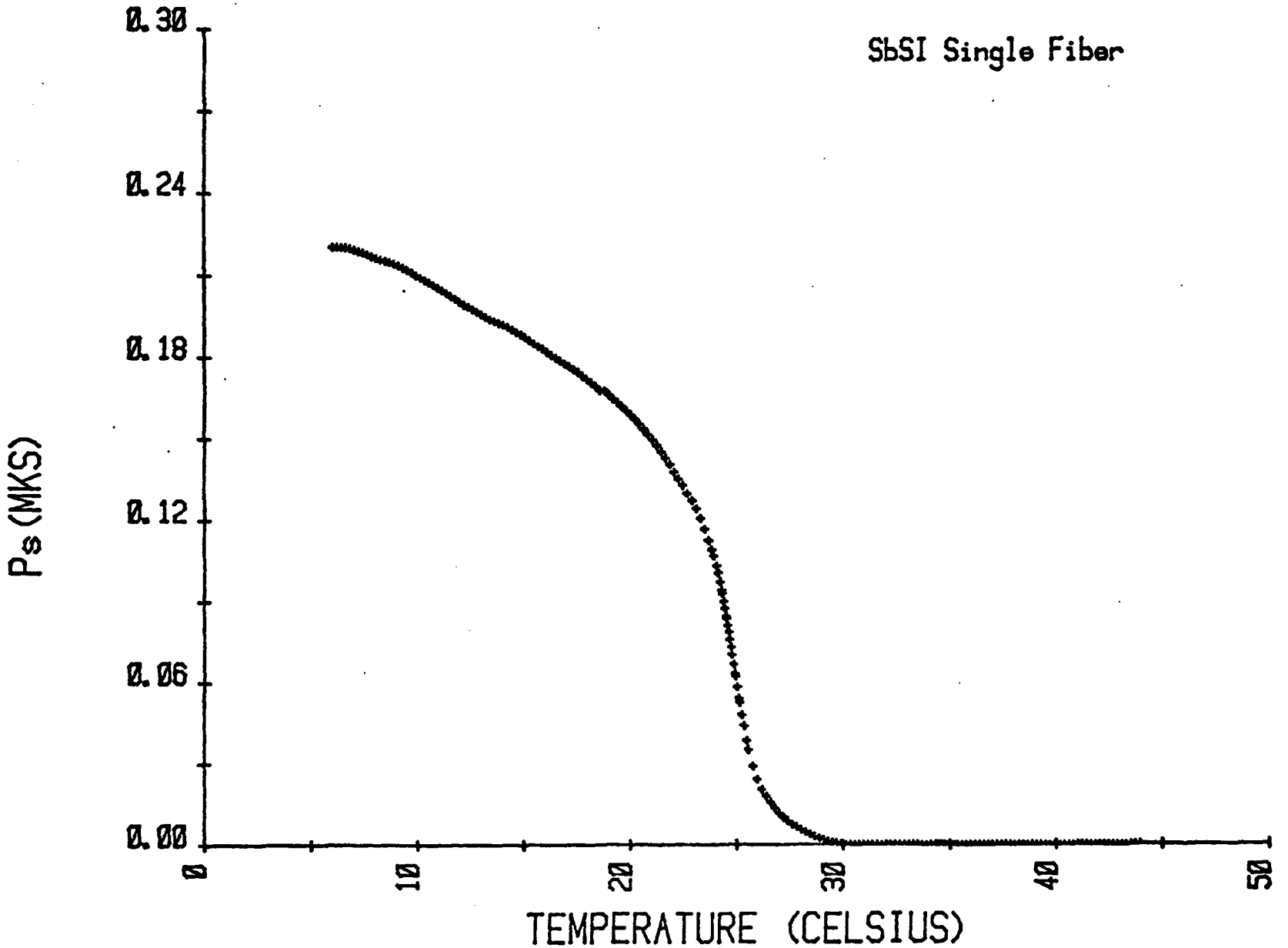
SbSI Single Fiber
0.30
0.24
0.18
0.12
0.06
0.00
Ps (MKS)
0
10
20
30
40
50
TEMPERATURE (CELSIUS)

Figure 5

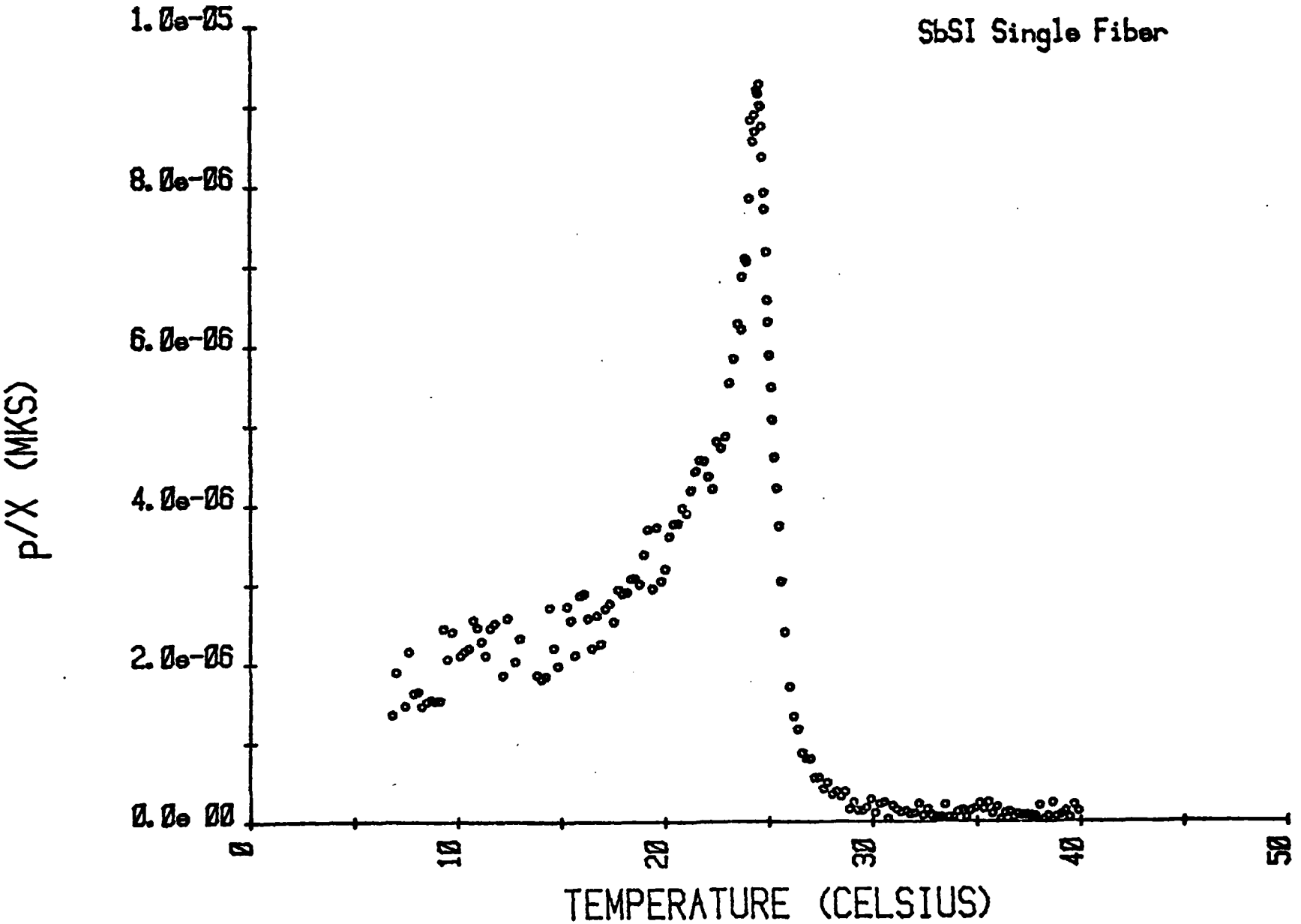
SbSI Single Fiber
1.0e-05
8.0e-06
6.0e-06
4.0e-06
2.0e-06
0.0e 00
P/X (MKS)
0
10
20
30
40
50
TEMPERATURE (CELSIUS)

Figure 6

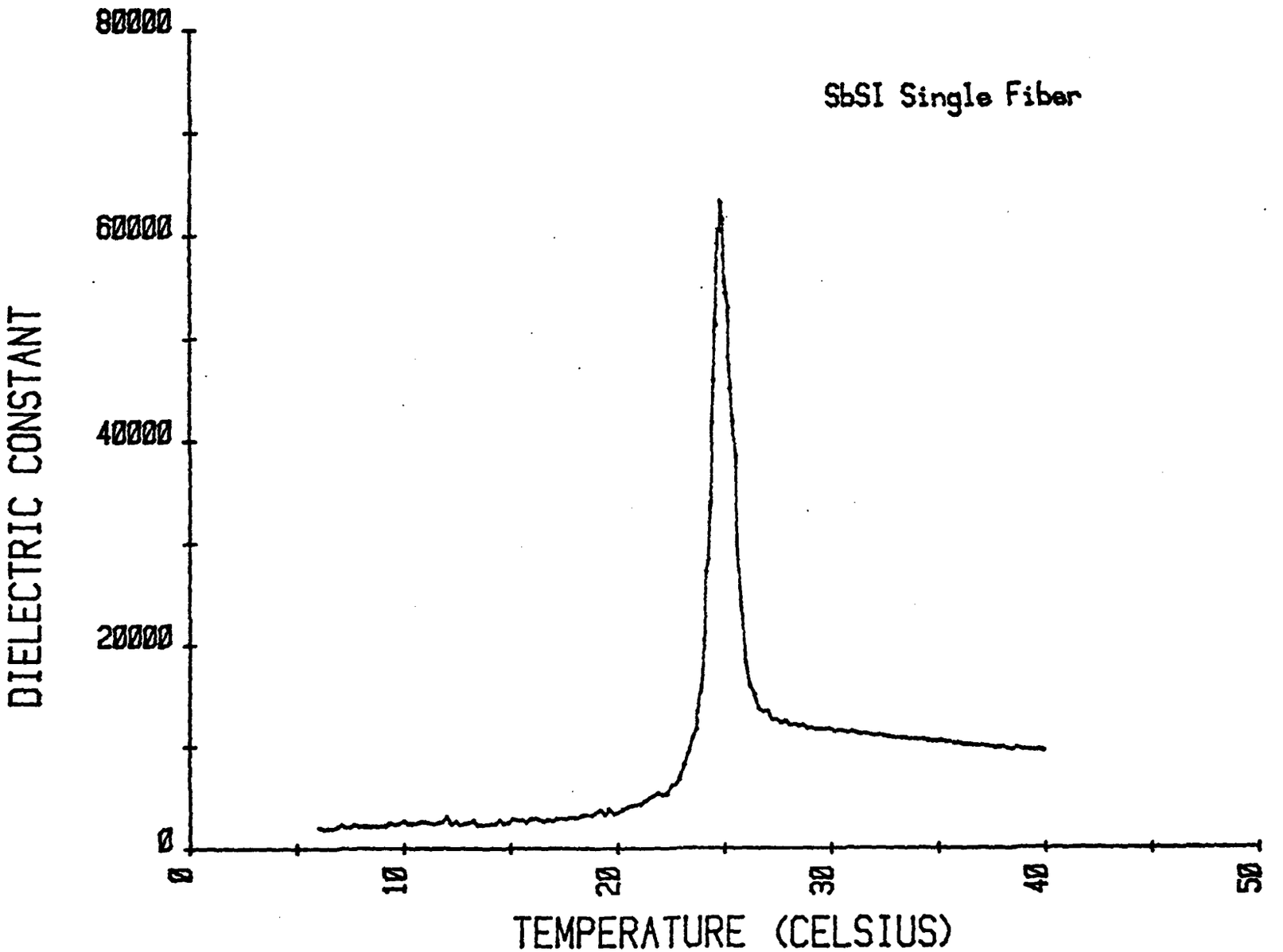
SbSI Single Fiber
DIELECTRIC CONSTANT
80000
60000
40000
20000
0
0
10
20
30
40
50
TEMPERATURE (CELSIUS)

Figure 7

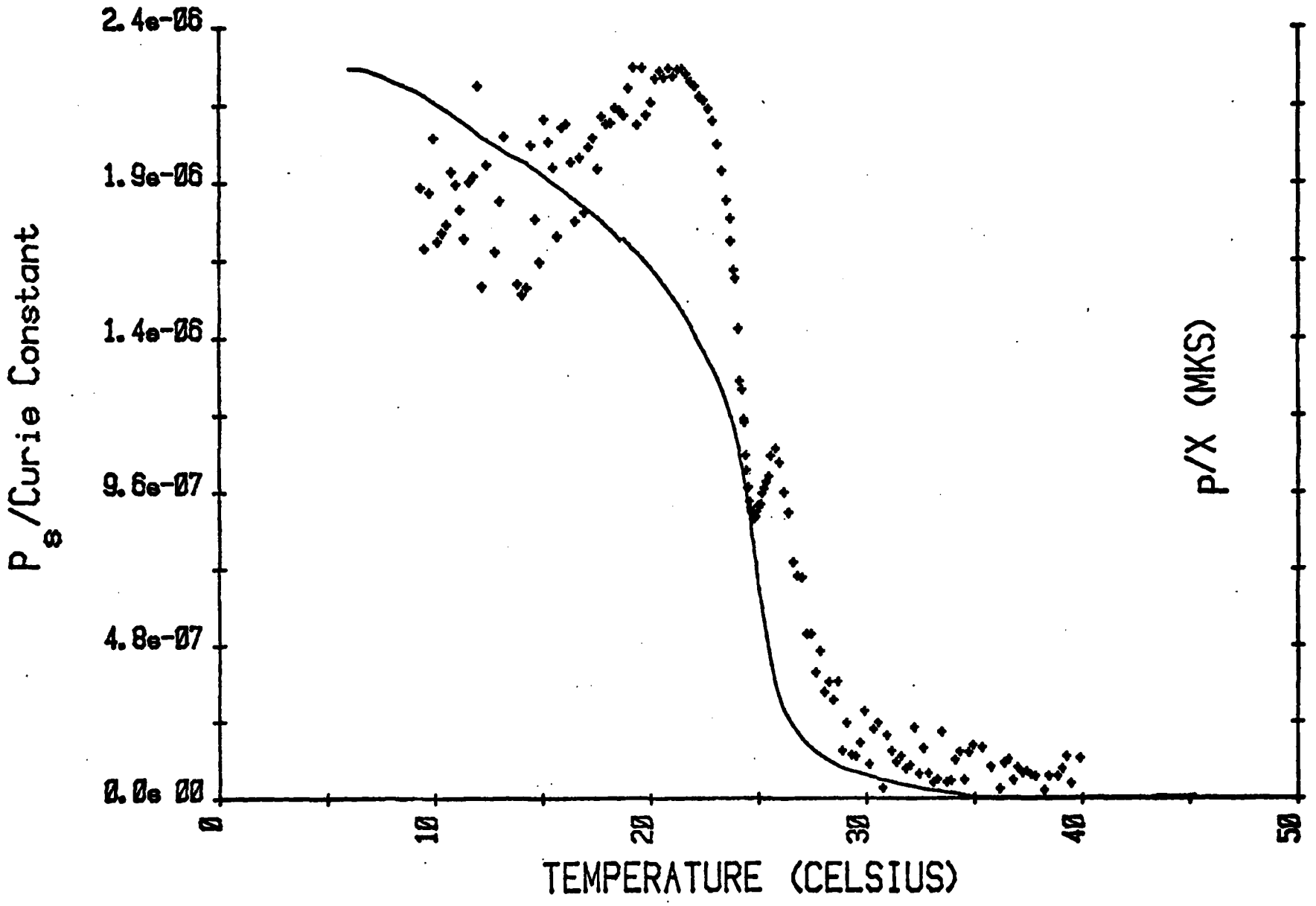
2.4e-06
1.9e-06
1.4e-06
9.6e-07
4.8e-07
0.0e 00
P_s/Curie Constant
p/X (MKS)
0
10
20
30
40
50
TEMPERATURE (CELSIUS)

Figure 8

APPENDIX III

Ferroelectric Ceramic-Plastic Composites for Piezoelectric and Pyroelectric Applications

R.E. Newnham, D.P. Skinner, K.A. Klicker, A.S. Bhalla,
B. Hardiman and T.R. Gururaja

FERROELECTRIC CERAMIC-PLASTIC COMPOSITES FOR PIEZOELECTRIC AND PYROELECTRIC APPLICATIONS

R.E. NEWNHAM, D.P. SKINNER, K.A. KLICKER, A.S. BHALLA,
B. HARDIMAN and T.R. GURURAJA
Materials Research Laboratory
The Pennsylvania State University
University Park, Pennsylvania 16802

Consideration of the influence of crystal symmetry, macrosymmetry, and interphase connectivity have been used to explore possible macrostructures of interest as piezoelectric or pyroelectric composites. Based on these design considerations, ceramic-plastic composites have been fabricated with 3-3 phase connectivity by the replication of natural template structures such as coral. Composites prepared in this way have piezoelectric g_{33} and g_h coefficients more than an order of magnitude higher than the coefficients of the homogeneously poled ferroelectric ceramic. Large voltage coefficients were also obtained from 3-1 piezoelectric composites made by embedding PZT fiber arrays in epoxy cement. Processing methods are described for producing straight and helical piezoelectric fibers by both extrusion and casting of PZT slips. Pyroelectric measurements on ceramic-plastic composites led to two interesting results: thermal expansion mismatch between the two phases can couple to the piezoelectric coefficients to give a large secondary pyroelectric effect, and, secondly, boracite-plastic composites have extremely large voltage coefficients (p/ε), comparable to boracite single crystals and the very best vidicon materials.

INTRODUCTION

Progress in materials science—like progress in most fields—follows the curve of history (Fig. 1). When a new effect such as ferroelectricity is discovered, scientific development is rather slow at first, until its importance is recognized. Then follows a period of rapid growth when practical applications and many new materials are discovered. Rapid changes take place in selecting the "best" material for each application. Eventually the field matures as the choices are made, and the curve of history saturates.

We see this saturation effect in many fields of materials science. PZT has been the best transducer material for 25 years. $BaTiO_3$ has been the best high K capacitor material for 30 years. Similar trends can be noted in magnetic materials, semiconductors, and superconductors. Despite intensive search for new compounds, relatively little progress has been made in the past ten or twenty years.

Where then do we go from here? Heterogeneous systems optimized for particular applications are certainly one possibility. Examples include semiconductor integrated circuits, fiber-reinforced metals, and barrier-layer ferroelectric capacitors. For the past three years we have been investigating some piezoelectric and pyroelectric composites, hoping to improve some of the properties of homogeneous materials. A summary of the basic ideas was published last year.[1] Connectivity is a critical parameter in composites designed for use as piezoelectric transducers or as pyroelectric detectors.

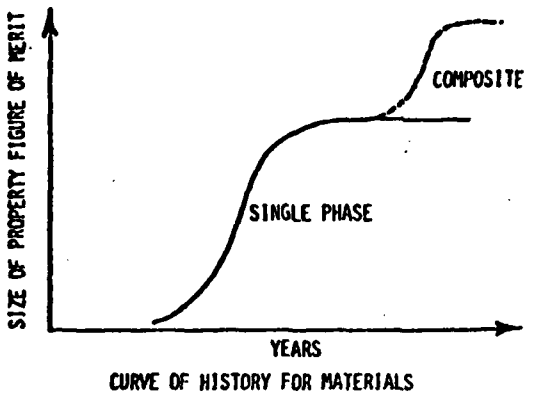

CURVE OF HISTORY FOR MATERIALS

Fig. 1

There are ten connectivity patterns in diphasic solids, ranging from a 0-0 unconnected checkerboard pattern to a 3-3 intertwined skeleton pattern in which both phases are three-dimensionally self-connected.

When the two phases are connected in parallel, the longitudinal piezoelectric voltage coefficient is

$$\bar{g} = \frac{v_I d_I s_{II} + v_{II} d_{II} s_I}{(v_I s_{II} + v_{II} s_I)(v_I \epsilon_{II} + v_{II} \epsilon_I)} \qquad (1)$$

In this expression, v_I and v_{II} are the volume fractions of the two phases. The piezoelectric coefficient, elastic compliance, and electric permittivity are represented by d, s, and ϵ, respectively. The composite of interest here is a mechanically stiff ferroelectric (phase I) in parallel with a soft compliant polymer (phase II), then $d_I >> d_{II}$, $s_I << s_{II}$, $\epsilon_I >> \epsilon_{II}$, and $\bar{g} \simeq d_I/v_{II}\epsilon_I$. Thus the voltage coefficient of the composite can easily exceed that of the solid ferroelectric.

In this paper we describe some processing methods for making 3-3 and 3-1 connectivity patterns which place the two phases in parallel. The composites give large voltage coefficients, as predicted by the theory.

A number of other research groups are also investigating the properties of ferroelectric composites with interesting connectivity patterns. Among the papers presented at this conference, there are examples of 3-0, 3-1, 3-3, and 2-2 patterns. The flexible PZT-polymer films described by Liu and Harrison[2] are 3-0 structures altered to 3-1 by grinding, while the properties of a ladder-type structure with 3-3 connectivity were reported by Miyashita and coworkers[3]. The internally electroded PZT multilayers investigated by Bowen and coworkers[4] are an excellent example of a metal-ceramic composite with 2-2 connectivity.

REPLAMINE TRANSDUCERS

Theoretical calculations indicate that a composite with 3-1 connectivity will have the best voltage coefficients, but 3-3 connectivity offers certain advantages in sample preparation; interconnections between the PZT fibers maintain the fiber orientation during the ceramic processing steps. In a 3-3 composite, both phases are self-connected in all these directions. Microstructures of this type occur in foams, phase-separated glasses, wood, and coral.

Coral skeletons are characterized by a narrow channel size distribution with complete interconnectivity. In the goniopera coral used in this study, the largest channel diameters are about 600 μm.

FERROELECTRIC CERAMIC-PLASTIC COMPOSITES

A lost-wax technique has been developed to replicate skeletal structures in other materials.[5,6] As illustrated in Fig. 2, the first step is to machine the coral in the desired shape. Using vacuum suction, the coral template is then impregnated with Kerr Inlay casting wax, after which the $CaCO_3$ skeleton is dissolved away in hydrochloric acid. The wax negative is reinvested with a PZT slip (43 volume% PZT, 53% H_2O, 4% poly (vinyl alcohol)). Ultrasonics PZT-501A with an average grain size of 1.6 μm was used in the process. The wax negative was burned off at 300°C, leaving a coral replica of PZT which was then sintered at 1280°C for one hour. The PZT replica was later back-filled with a high-purity silicone rubber (Dow Corning MDX-4-4210 Elastomer). After attaching silver-loaded silicone rubber electrodes, the composite was poled for five minutes at 100°C under an electric field of 14 kV/cm.

As poled, the PZT-rubber replica is mechanically rigid, but flexing the composite fractures the ceramic skeleton and improves the piezoelectric properties. Shearing the structure lowers the permittivity without appreciably affecting the piezoelectric d coefficient. As a result, the longitudinal voltage coefficient g_{33} is greatly enhanced.

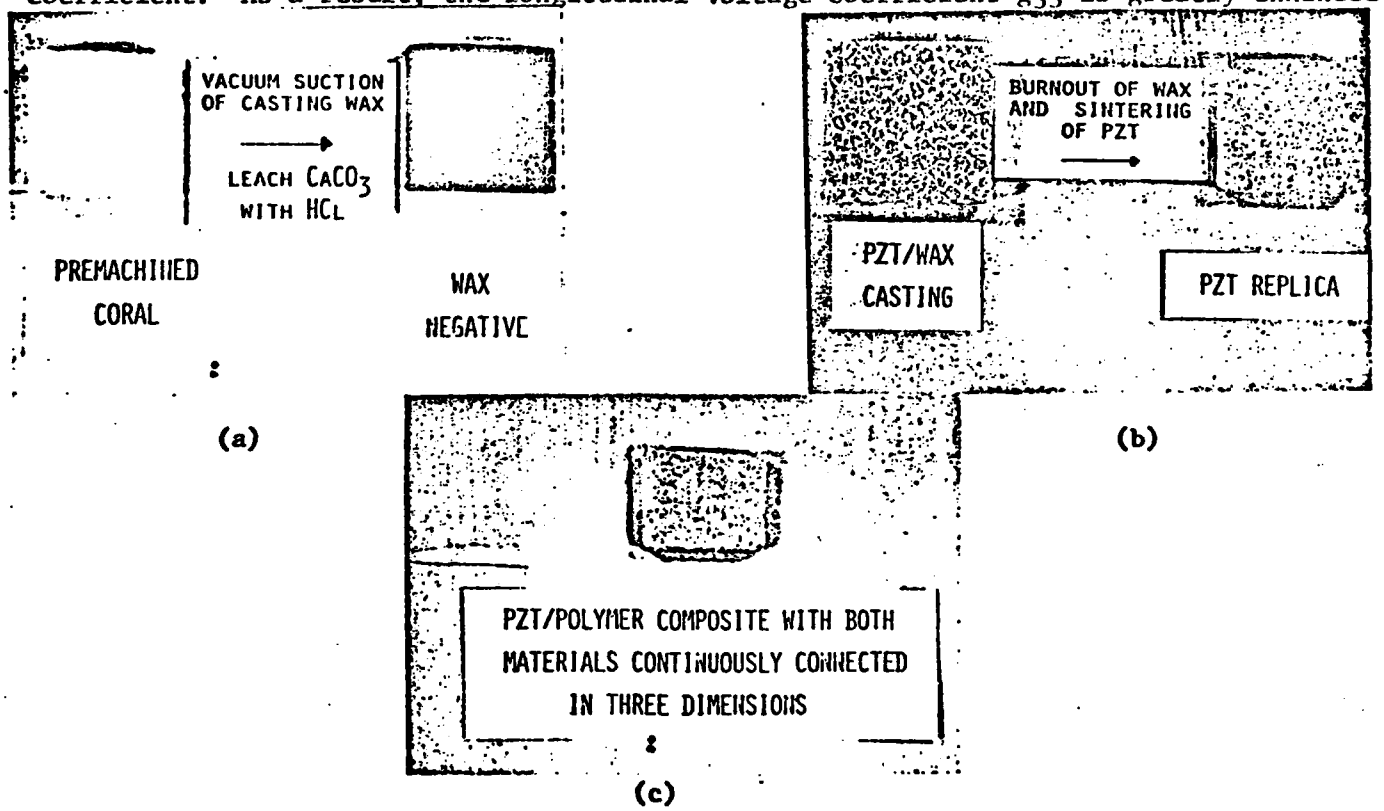

Fig. 2 A lost-wax technique to replicate skeletal structures.

The measured values are $K_{33} = 40$, $d_{33}=100\times10^{-12}$ C/N, and $g_{33} = 300\times10^{-3}$ Vm/N, about fifteen times better than a solid PZT ceramic of similar composition. Three other advantageous properties of the composite are low density, high felxibility, and high tensile strength.

PIEZOELECTRIC FIBERS IN PLASTIC

Composites with 3-1 connectivity have been made by aligning PZT rods in a plastic matrix. In the 3-1 model (eq 1), the piezoelectric effect of the composite depends on the volume fractions of the constituent phases, together with their permittivities,

piezoelectric coefficients, and elastic compliances. By varying the spacing between the PZT rods and their diameters, the conditions maximizing $\bar{d}_{33}$ and $\bar{g}_{33}$ are under study.

PZT rods are formed by extruding a slip of commercial PZT[a] in a PVA solution. The slip composition was 90 wt% PZT, 8% water, 2% PVA. Using dies of several different diameters, the slip was extruded onto a moving glass plate to ensure straightness of the green PZT rods. After drying for 24 hours at room temperature, the rods were cut into 35 mm segments and sintered at 1305°C for a half-hour.

Initially, the PZT rods proved difficult to pole because of air bubbles introduced during extrusion. To reduce the porosity and increase the electric breakdown strength, the sintered rods were refired in a hot isostatic press (HIP) for one hour at 1300°C under a 200 atmosphere pressure of argon. The final density was 7.82 g/cm^3. Rods of 0.84 mm diameter were used in the piezoelectric measurements, but thinner PZT rods of 0.66, 0.46, and 0.20 mm diameter have been produced by the same method.

A pair of brass disks with drilled holes were used to align the piezoelectric rods in parallel arrays (Fig. 3a). Four racks were made with different hole separations to give composites with 50, 40, 30, and 20 volume percent PZT. After alignment, the rack and rods were placed in a closed plastic tube and embedded in Spurrs epoxy[b]. Following a setting time of 16 hours at 70°C, the composite slug was sliced into disks with a diamond saw (Fig. 3b). Poling was carried out in an oil bath at 75°C by applying a field of 22 kV/cm for five minutes.

According to our theoretical model for parallel connectivity[1], the d_{33} coefficient for the composite is approximately equal to the d_{33} value of the piezoelectric phase if the piezoelectric is mechanically stiffer than the second phase. As long as the piezoelectric phase acts as the force-bearing component of the composite, $\bar{d}_{33}$ will be independent of volume fraction. Figure 4 shows the measured values for the PZT-Spurrs composites with 3-1 connectivity. The $\bar{d}_{33}$ values were measured with a Berlincourt d_{33} meter[c] using flat metal plates on the surfaces of the samples to distribute the weight evenly. As predicted by the model, the measured d_{33} values are independent of volume fraction, but are only about 75% of the d_{33} value of PZT 501A ceramic. This discrepancy may be due to incomplete poling of the rods, or perhaps to the approximations involved in the theory.

Electric permittivity and piezoelectric voltage coefficients are also plotted in Fig. 4. For idealized parallel connectivity, the permittivity of a diphasic composite is $v_I\varepsilon_I + v_{II}\varepsilon_{II}$, where v_I and V_{II} are the volume fractions of the two constituent phases with permittivities ε_I and ε_{II}. Since the dielectric constant of PZT ($\sim$ 2000) is much larger than that of Spurrs ($\sim$4), the dielectric constant of the composite is about 2000 v, where v is the volume fraction of PZT. This expression agrees well with the measurement.

The piezoelectric voltage coefficient g is defined as d/ε. Voltage coefficients for the PZT-Spurrs composites increase rapidly at low volume fractions of PZT because of the decrease in permittivity. Measured g values for the composite with 20% PZT were about 3.5 times larger than solid PZT.

Experiments are now underway with smaller volume fractions of PZT and with helical fibers (Fig. 3c). When arranged in bedspring arrays, the PZT spirals show some interesting piezoelectric effects. The helices were made in two ways: by extrusion and by casting. The extrusion technique is a variation on the method described earlier for making straight PZT rods. Immediately following extrusion, the green fibers were wrapped around a plastic mandrel to form spirals. After drying, the coils were slipped off the mandrel and sintered at 1300°C for 30 minutes in an alumina crucible. To protect the coils during sintering, they are buried in coarse PZT powder.

---

[a]PZT 501A, Ultrasonic Powders, Inc., South Plainfield, NJ 07080.
[b]Ernest F. Fullam, Inc., Schenectady, NY 12301.
[c]Channel Products, Inc., Chagrin Falls, Ohio 44022.

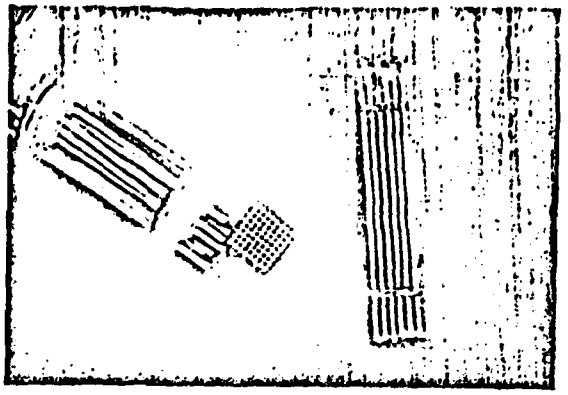

(a)

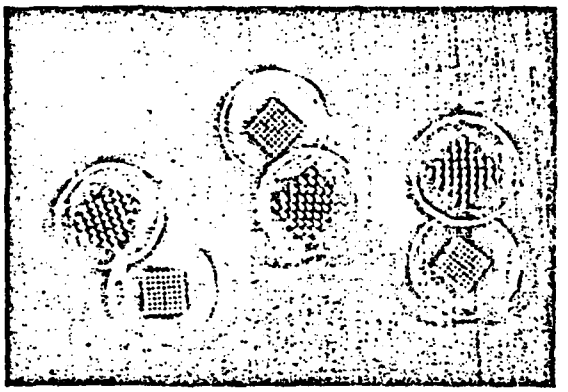

(b)

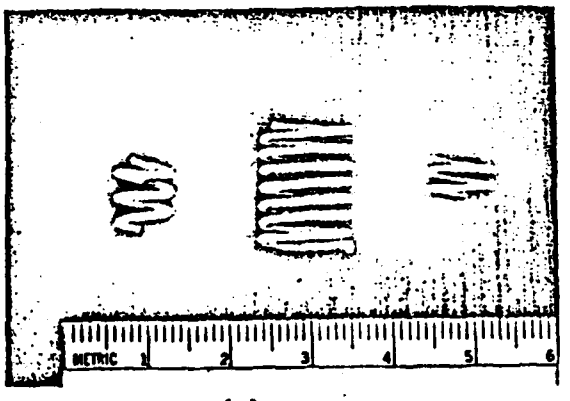

(c)

Fig. 3 (a) Alignment of the piezoelectric rods in parallel arrays for the composites with 3-1 connectivity. (b) PZT:SPURRS composite discs with various volume percent PZT. (c) Helical fibers made of PZT.

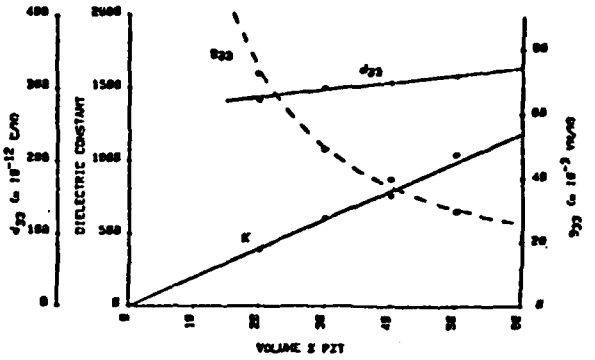

Fig. 4 Plots of K, d_{33} and g_{33} versus volume % PZT.

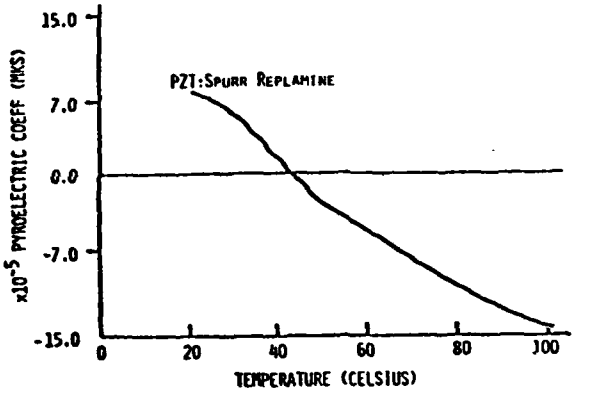

Fig. 5 Temperature dependence of the piezoelectric response in a PZT: SPURRS composite.

Spirals with rectangular cross-sections were made by casting. A metal template was made by machining a spiral groove on the surface of a solid cylindrical rod. The template was then inserted in a hollow cylindrical tube fitted with end pieces. The metal tube was then partially filled with PZT 501 slip and then centrifuged for five minutes at 3500 RPM. The template and cast ceramic were removed from the holder and partially dried. Removal of the green ceramic helix from the template was accomplished by inserting the template into a hollow cylinder and unscrewing the template through a blocking pin, leaving the ceramic coil inside the cylinder. The coil was allowed to dry for 24 hours and then fired by the usual procedure.

PYROELECTRIC COMPOSITES

During the past year we have also been studying pyroelectric composites, seeking to maximize the figure of merit p/ε for vidicon applications[1] for simple model systems suggest that two phase systems with suitably chosen connectivity patterns can have pyroelectric coefficients larger than either individual phase. Two pyroelectric materials connected in parallel have a composite pyroelectric coefficient

$$\bar{p} = v_I p_I + v_{II} p_{II} + \frac{v_I v_{II} (\alpha_{II} - \alpha_I)(d_I - d_{II})}{v_I s_{II} + v_{II} s_I}$$

where v_I and v_{II} are the volume fractions of the two phases and p, α, d, and s represent their pyroelectric, thermal expansion, piezoelectric, and elastic compliance coefficient The secondary pyroelectric effect makes a major contribution whenever there is an appreciable thermal expansion mismatch between the two phases.

Pyroelectric measurements have been carried out on the PZT-plastic composites used in the piezoelectric experiments. Even though PZT is far from ideal as a pyroelectric, it can be used in model systems to test different composite geometries. Current studies on the PZT based materials are concerned with validating the measurement procedures, ascertaining the optimum connectivity, and exploring the influence of the scale of the heterogeneity in relation to the sample dimensions.

So far we have succeeded in demonstrating that PZT-Spurrs composites fabricated by the replamine technique improves the pyroelectric figure of merit p/ε by a factor of 6 over that of solid PZT. The temperature dependence of the pyroelectric response exhibits an interesting compensation point where the primary and secondary effects cancel out (Fig. 5). AT room temperature the hard plastic mechanically clamps the PZT, but at higher temperatures the plastic softens. PZT-soft polymer composites showed no enhancement of the pyroelectric figure of merit. Major changes in the pyroelectric response were noted when the sample thickness was comparable to the scale of the composite heterogeneity.

BORACITE COMPOSITES

Improper ferroelectrics such as the boracites ($M_3B_7O_{13}X$: M=Cu,Ni,Co,Fe,Mn; X=Cl, Br,I) possess unusual property coefficients, including a large figure of merit for pyroelectric vidicon applications.[7] The pyroelectric voltage coefficients of $Cu_3B_7O_{13}Cl$, $Ni_3B_7O_{13}Br$ and $Fe_3B_7O_{13}I$ are larger than that of deuterated triglycine fluoberyllate (DTGFB), but a number of problems remain to be solved before boracite crystals can be used for vidicon targets. Crystals larger than a few millimeters of acceptable chemical homogeneity and free from fracture are very difficult to grow and pole.

FERROELECTRIC CERAMIC-PLASTIC COMPOSITES

Boracite-plastic composites appear to be an attractive alternative to the single crystals. Some preliminary measurements were made using $Fe_3B_7O_{13}I$ crystallites obtained from the Plessey Company. The tiny crystals were crushed and screened between 100 and 200 mesh and then mounted in a Spurrs epoxy film. We found that the films became strongly pyroelectric after poling and that the signal level increases with the degree of poling. The figure of merit of the composites was the same as that of Fe-I boracite single crystals.

There are two excellent reasons why the boracite composites pole so easily: first, the dielectric constant of boracite is about the same as the plastic, and second, boracite has twelve domain orientations, far more than most ferroelectrics. Based on these encouraging results, it seems worthwhile to develop processing techniques for boracite composites and polycrystalline aggregates for pyroelectric applications.

ACKNOWLEDGMENTS

The boracite crystals used in the pyroelectric composites were supplied by Dr. Roger Whatmore of the Plessey Co. Some of the pyroelectric measurements were carried out in cooperation with Dr. Joseph Dougherty and Dr. Wallace Smith of the North American Philips Laboratories. The advice and assistance of our colleagues at Penn State and Dr. Robert Pohanka of the Naval Research Laboratory are also acknowledged with gratitude. This work was sponsored by the Department of Defense through contracts N00014-78-C-0291 and MDA 903-78-C-0306.

REFERENCES

1. R.E. Newnham, D.P. Skinner, L.E. Cross, Mat. Res. Bull. 13, 525 (1978).
2. S.T. Liu and W.B. Harrison, Ferroelectrics (this issue).
3. M. Miyashita, K. Takano, T. Toda, Ferroelectrics (this issue).
4. L. Bowen, T. Shrout, W. Schulze, J.V. Biggers, Ferroelectrics (this issue).
5. R.A. White, J.N. Weber, E.W. White, Science, 176, 922 (1972).
6. D.P. Skinner, R.E. Newnham, L.E. Cross, Mat. Res. Bull. 13, 599 (1978).
7. R.W. Whatmore, C.J. Brierley and F.W. Ainger, Ferroelectrics (this issue).